1   **Retinoblastoma binding protein 4 maintains cycling neural stem cells and prevents DNA**

2   **damage and Tp53-dependent apoptosis in *rb1* mutant neural progenitors**

3

4

5   Laura E. Schultz-Rogers[1,2], Maira P. Almeida[1], Wesley A. Wierson[1], Marcel Kool[3,4] and Maura

6   McGrail[1]*

7

8   [1] Department of Genetics, Development and Cell Biology, Iowa State University, Ames, IA

9   50011, USA.

10   [2] Present address: Center for Individualized Medicine, Mayo Clinic, Rochester, MN 55905, USA

11   [3] Hopp Children's Cancer Center at the NCT (KiTZ), 69120 Heidelberg, Germany

12   [4] Division of Pediatric Neuro-oncology, German Cancer Research Center (DKFZ), and German

13   Cancer Consortium (DKTK), 69120 Heidelberg, Germany

14

15

16   * Correspondence: mmcgrail@iastate.edu

17

18   Short Title: Rbbp4 in neural stem cell maintenance and neural progenitor genome integrity

19

20

21

Abstract

Retinoblastoma-binding protein 4 (Rbbp4) is a WDR adaptor protein for multiple chromatin remodelers implicated in human oncogenesis. Here we show Rbbp4 is overexpressed in zebrafish *rb1*-embryonal brain tumors and is upregulated across the spectrum of human embryonal and glial brain cancers. We demonstrate *in vivo* Rbbp4 is essential for zebrafish neurogenesis and has distinct roles in neural stem and progenitor cells. *rbbp4* mutant neural stem cells show delayed cell cycle progression and become hypertrophic. In contrast, *rbbp4* mutant neural precursors accumulate extensive DNA damage and undergo programmed cell death that is dependent on Tp53 signaling. Loss of Rbbp4 and disruption of genome integrity correlates with failure of neural precursors to initiate quiescence and transition to differentiation. *rbbp4; rb1* double mutants show that survival of neural precursors after disruption of Rb1 is dependent on Rbbp4. Elevated Rbbp4 in Rb1-deficient brain tumors might drive proliferation and circumvent DNA damage and Tp53-dependent apoptosis, lending support to current interest in Rbbp4 as a potential druggable target.

44 ## Author Summary

45

46 Examining the developmental mechanisms controlling neural stem and progenitor cell behavior

47 is critical to our understanding of the processes driving brain tumor oncogenesis. Chromatin

48 remodelers and their associated adaptor proteins are thought to be key drivers of brain

49 development and disease through epigenetic regulation of gene expression and maintenance of

50 genome integrity, but knowledge of their *in vivo* roles in vertebrate neurogenesis is limited. The

51 chromatin remodeler adaptor protein Rbbp4 has recently been shown to function in a mouse

52 model of neuroblastoma and in glioblastoma multiforme cell resistance to the chemotherapeutic

53 temozolomide. However, an *in vivo* requirement for Rbbp4 in neurogenesis has only just been

54 shown by isolation of a recessive lethal mutation in zebrafish *rbbp4*. Here we provide conclusive

55 genetic evidence that zebrafish rbbp4 is essential in neural stem and progenitor cell function

56 during development. Our data reveal for the first time *in vivo* that Rbbp4 prevents DNA damage

57 and activation of Tp53 signaling pathway that leads to programmed cell death. Importantly,

58 neural progenitors that are mutant for the tumor suppressor Rb1 also depend on Rbbp4 for

59 survival. Finally, we show that neural stem cells that have lost Rbbp4 cease dividing, and may

60 enter a senescent like state. Together, these observations provide novel evidence that elevated

61 expression of Rbbp4 in *rb1*-mutant tumors may contribute to cancer cell survival by blocking

62 senescence and/or DNA damage-induced cell death.

63

64

65

66

3

Introduction

The Retinoblastoma Binding Protein 4 (RBBP4) is a WD40 Repeat (WDR) protein that functions as a chromatin assembly factor and adaptor for multiple chromatin remodelers regulating gene expression and DNA repair. RBBP4 associates with chromatin through histone H3 and H4 binding sites on the surface and side of the β-propeller, respectively (1-3). These locations are potential sites for chemical inhibitors of RBBP4 activity (4). RBBP4 is a component of the H3K27methyltransferase polycomb repressive complex PRC2 (2) and the nucleosome remodeling and histone deacetylase complex NuRD (5-7) and binds the histone acetyltransferase p300/CREB binding protein complex (8). RBBP4-dependent recruitment of chromatin regulators has recently been shown to control glioblastoma multiforme cell resistance to temozolomide through p300 activation of DNA repair pathway genes (9), and tumor progression in neuroblastoma xenografts by PRC2 silencing of tumor suppressors (10). Only recently has an *in vivo* requirement for RBBP4 in vertebrate development and neurogenesis been demonstrated by mutational analysis in zebrafish (11). Given the importance of understanding how developmental mechanisms contribute to the cellular and molecular basis of cancer (12), a more detailed examination of the role of RBBP4 in neural development would provide additional knowledge into its possible oncogenic roles in brain tumors.

RBBP4 was first discovered as a binding partner of the tumor suppressor RB1 in yeast (13) and studies in *C.elegans* revealed the RBBP4 homolog *lin-53* negatively regulates vulval precursor cell fate by repression of genes required for vulval induction (14). Drosophila and human RBBP4 were shown to be a component of the RB1-like DREAM complex, which binds E2F target gene promoters to repress cell cycle gene expression and promote entry into quiescence (15). These early *in vivo* studies indicated RBBP4 functions in cell cycle progression and cell fate specification through transcriptional regulation by RB family members. RB1 has been well studied in mouse and shown to be essential for embryonic and adult neurogenesis (16, 17). Zebrafish *rb1* is also an essential gene required for neural development (18, 19). Mutant analysis plus live brain imaging revealed zebrafish *rb1* mutant neural progenitors reenter the cell cycle and fail to progress through mitosis, whereas loss of *rbbp4* induces neural progenitor apoptosis (11). Together these studies suggest Rbbp4 and Rb1 cooperate to ensure neural progenitor cell cycle exit and differentiation.

4

99   In this study we use developmental genetics to further investigate the *in vivo* role of

100   Rbbp4 in zebrafish neurogenesis and examine the interaction of Rbbp4 and Rb1 in neural

101   progenitor cell fate. Rbbp4 is enriched in zebrafish neural stem and precursor cells during

102   development and in adult brain. Rbbp4 is also upregulated across many human embryonal and

103   glial brain tumors. We find that *rbbp4* mutant neural stem cells become hypertrophic, while

104   neural precursors accumulate DNA damage and undergo Tp53-dependent apoptosis. *in situ*

105   analysis demonstrates *rbbp4* mutant progenitors are lost before exiting the cell cycle and

106   initiating the G0 gene expression program. Double mutant analysis shows Rbbp4 is required for

107   the survival of *rb1*-mutant neural progenitors. Our developmental analyses suggest a potential

108   oncogenic role for Rbbp4 in *rb1*-defective brain cancer cells by promoting proliferation and

109   preventing DNA damage induced apoptosis.

110

111

112

113   **Results**

114

115   **Rbbp4 protein is expressed in zebrafish adult neural stem/progenitors and in *rb1-***

116   **embryonal brain tumors**

117

118   We previously showed by RNA-Seq and qRT-PCR that *rbbp4* is overexpressed in

119   zebrafish *rb1*-brain tumors, and demonstrated it is required in neural development by isolating a

120   larval lethal homozygous mutant allele *rbbp4^{Δ4is60}* (11). Here we used a commercially available

121   antibody to examine Rbbp4 localization in zebrafish tissues. Western blotting with the anti-

122   RBBP4 polyclonal antibody detects a single band of ~47 kDa in whole protein extract from 5 day

123   post fertilization (dpf) wildtype zebrafish larvae that is absent in *rbbp4^{Δ4/Δ4}* homozygous mutant

124   extract (Fig S1A). In cross sections of 5 dpf head tissue Rbbp4 labeled nuclei are detected

125   throughout the brain, but the labeling was again absent in *rbbp4^{Δ4/Δ4}* homozygous mutant tissue

126   (Fig S1B, S1C), confirming the specificity of the antibody. In wild type adult zebrafish, stem and

127   progenitor cells line the ventricle and subventricular zone of midbrain structures (Fig 1A). Rbbp4

128   is detected in cells lining the midbrain ventricle where stem cells reside (Fig 1B-D) and is

129   enriched in the nuclei of cells with high levels of proliferating cell marker PCNA (Fig 1D arrow).

130   Rbbp4 was also present in nuclei of cells throughout the midbrain peri-granular zone (Fig 1E). In

131   *rb1*-brain tumor tissue (Fig 1F) high levels of nuclear Rbbp4 were detected in cells throughout

132 the lesion (Fig 1G) that frequently co-labeled with PCNA (Fig 1H, 1I). These results confirm

133 overexpression of Rbbp4 protein in zebrafish *rb1*-brain tumors, as predicted by our previous

134 RNA-Seq analysis (11).

135

136

Human RBBP4 is upregulated across the spectrum of aggressive brain cancers

138

139 We examined expression data from 2284 human brain tumor samples (German Cancer

140 Research Center) to determine if *RBBP4* is upregulated in human embryonal tumors and other

141 aggressive brain cancers. Molecular profiling has classified human embryonal central nervous

142 system primitive neuroectodermal tumors (CNS-PNETs) into major groups with distinct

143 molecular subtypes (20-22). *RBBP4* was upregulated across all embryonal tumors and

144 subtypes (Fig 1J) as well as in ependymal, glial, oligodendroglial and astrocytic tumors (Fig

145 S1D). Together these results indicate elevated *RBBP4* may be a common signature in

146 aggressive central nervous system tumors.

147

148

Zebrafish Rbbp4 protein is ubiquitously localized in embryonic neuroblasts and
varies in neural cell populations in the larval midbrain

151

152 Rbbp4 expression was examined in the 2 dpf embryonic (Fig 2A, 2B) and 5 dpf larval

153 (Fig 2C, 2D) wildtype zebrafish developing brain. At 2 dpf nuclear Rbbp4 is present in all neural

154 precursor cells throughout the midbrain and retina and co-labels with proliferating cell marker

155 PCNA (Fig 2E, 2F, S2). Rbbp4 and PCNA were highly enriched in neural stem cells lining the

156 midbrain ventricle (Fig 2G) and at the ciliary marginal zone (CMZ) of the retina (Fig 2H). The

157 end of 2 dpf marks the transition from embryonic to larval neurogenesis and growth in the brain

158 becomes asymmetric (23, 24). By 5 dpf, proliferative zones are confined to the midbrain

159 ventricles and dorsal tectum and the retinal ciliary marginal zone (25, 26). In the 5 dpf midbrain

160 (Fig 5I) Rbbp4 is significantly reduced or absent from most cells in the proliferative zones (Fig

161 2J, 2K and 2H outlined areas; Fig S3) but is detectable in PCNA-positive cells (Fig 2K and 2L

162 arrows; Fig S3). Varying levels of Rbbp4 were present in cells adjacent to the ventricle and in

163 neurons throughout the parenchyma. At 5 pdf the retina is laminated into 3 distinct nuclear

164 layers and stem cells and progenitors are restricted to the ciliary marginal zone (Fig 2M). Rbbp4

165 is detectable in PCNA-positive cells at the retinal ciliary marginal zone (Fig 2N and 2O outlined

166   area, Fig S3). In the central retina, high levels of Rbbp4 were restricted to neurons in the

167   ganglion cell layer and at the vitreal side of the inner nuclear layer (Fig 2P, Fig S3). A low level

168   of Rbbp4 was detected in outer nuclear layer photoreceptors (Fig 2P). In summary, in the larval

169   midbrain and retina Rbbp4 is present in proliferating stem and progenitor cells and is elevated to

170   varying levels in other neuronal cell populations. This suggests a role for Rbbp4 in both neural

171   stem and precursor cells during brain development.

172

173

174   **Rbbp4 is essential for development of brain, eye and neural crest derived**

175   **structures**

176

177   Zebrafish larvae homozygous mutant for the 4 base pair frameshift mutation $rbbp4^{\Delta4}$

178   display severe defects in neurogenesis, presenting with microcephaly and microphthalmia (Fig

179   3A-3D). Alcian blue staining revealed several abnormalities in formation of head cartilage

180   structures (Fig 3E-3H), including the ceratohyal cartilage (ch), ceratobranchial cartilage (cbs),

181   and Meckel's cartilage (m). These results suggest that Rbbp4 is necessary for development of

182   the central nervous system and neural crest derived structures. Ubiquitous overexpression of

183    $rbbp4$ cDNA by a $Tol2<ubi:rbbp4-2AGFP>$ transgenic line (Fig 3I) was tested for the ability to

184   rescue the $rbbp4^{\Delta4/\Delta4}$ phenotype. The transgene did not affect development in wild type embryos

185   or viability and fertility in adults (Fig 3J, Table S1) and was able to rescue the gross

186   morphological defects in $rbbp4^{\Delta4/\Delta4}$ mutants (Fig 3K and Fig S3). Midbrain height and eye width

187   measurements in $Tol2<ubi:rbbp4-2AGFP>$ and $rbbp4^{\Delta4/\Delta4}$;$Tol2<ubi:rbbp4-2AGFP>$ transgenic

188   embryos confirmed rescued animals showed no significant difference in morphology from

189   wildtype (Fig 3L and 3M). $rbbp4^{\Delta4/\Delta4}$; $Tg(Tol2<ubi:rbbp4-2AGFP>)$ individuals are viable and

190   become fertile adults. These results demonstrate Rbbp4 is essential for larval viability, midbrain

191   and retina development, and formation of neural crest derived cartilage.

192

193

194   **Loss of Rbbp4 leads to stem cell hypertrophy and defects in midbrain**

195   **neurogenesis**

196

197   The effect of loss of Rbbp4 on specific neural cell populations in the 5 dpf larval midbrain

198   and retina was examined with proliferation, stem, neural, and glial markers (Fig 3N-3U, Fig S5).

7

199   In wildtype (Fig 3N) and *rbbp4*$^{\Delta4/\Delta4}$ mutant (Fig 3O) the stem/progenitor marker Sox2 was

200   present in cells lining the midbrain ventricle and adjacent to the ventral thalamus. Sox2 positive

201   cells were also scattered throughout the wild type dorsal tectum (Fig 3P bracket). The dorsal

202   tectum was dramatically reduced in *rbbp4*$^{\Delta4/\Delta4}$ and only low levels of Sox2 were detected (Fig

203   3Q bracket). Sox2-positive cells frequently co-labeled with PCNA at the midbrain ventricle in

204   wildtype (Fig 3P outline) and *rbbp4*$^{\Delta4/\Delta4}$ (Fig 3Q outline), however, the *rbbp4*$^{\Delta4/\Delta4}$ cells showed

205   an enlarged, hypertrophic morphology. In the retina, high levels of PCNA labeling was present

206   in stem cells at the ciliary marginal zone in both wildtype (Fig 3R) and *rbbp4*$^{\Delta4/\Delta4}$ (Fig 3S), but

207   the *rbbp4*$^{\Delta4/\Delta4}$ ciliary marginal zone was expanded and stem cells were enlarged and

208   hypertrophic (Fig 3T and 3U outlines), similar to cells in the midbrain ventricle. A gap of missing

209   tissue separated the ciliary marginal zone and the neural retina in the *rbbp4*$^{\Delta4/\Delta4}$ mutant (Fig 3U

210   arrow). These results suggest loss of Rbbp4 prevents brain and retina growth by disrupting

211   production and survival of neural precursors. Examination of the glial markers Gfap and Blbp

212   and neuronal markers synaptic vesicle Sv2 and Calretinin (Fig S5) revealed early neurogenesis

213   occurred normally in the *rbbp4*$^{\Delta4/\Delta4}$ mutant brain and retina. Maternal Rbbp4 may protect the

214   earliest born embryonic neural precursors, allowing them to migrate to their final location and

215   differentiate into mature neurons and glia in the brain and retina. Together, these results

216   indicate Rbbp4 is necessary for persistent production of neural precursors and their transition to

217   newborn neurons and glia.

218

219

220   **Rbbp4 is required to prevent persistent DNA damage and apoptosis in neural**

221   **precursor cells**

222

223   To determine if the defect in neurogenesis in 5 dpf *rbbp4*$^{\Delta4/\Delta4}$ mutant larva was due to

224   activation of programmed cell death earlier in the developing brain, we examined gross

225   morphology, apoptosis, and DNA damage in wildtype and *rbbp4*$^{\Delta4/\Delta4}$ brain and retina at 2 and 3

226   dpf. Compared to wildtype, at 2 and 3 dpf the size of the optic tectum (Fig 4 A-C, arrows, OT)

227   and midbrain-hindbrain structures (Fig E-H, brackets) was reduced in *rbbp4*$^{\Delta4/\Delta4}$ mutant larvae.

228   Apoptosis was examined by labeling sectioned tissue with an antibody to activated Caspase-3

229   and comparing the number of labeled cells between wildtype and *rbbp4*$^{\Delta4/\Delta4}$ mutants (Fig 4 I-P).

230   At 2 dpf in wildtype very few cells were labeled with activated Caspase-3, whereas labeling was

231   significantly increased and present throughout the *rbbp4*$^{\Delta4/\Delta4}$ tectum and overlapped with cells

232   containing fragmented nuclei throughout the retinal ganglion and inner nuclear layers (Fig 4I-

8

233   4L). At 3 dpf, few cells again were labeled in wildtype (Fig 4M). In $rbbp4^{\Delta 4/\Delta 4}$, the amount of

234   Caspase-3 labeling was reduced and was restricted to the proliferative zones in the dorsal

235   tectum and periphery of the retina (Fig 4N). Quantification of Caspase-3 labeled cells revealed

236   the increase in the $rbbp4^{\Delta 4/\Delta 4}$ mutant at 2 dpf was significant in the brain and retina (Fig 4O). At

237   3 dpf the difference was less significant (Fig 4P), possibly due to overall reduction in cell

238   number from programmed cell death or a decrease in production of new neural precursors.

239   Activated Caspase-3 positive cells at the retina periphery did not co-label with neuronal marker

240   HuC/D, and nuclei appeared fragmented or pyknotic (Fig S6). This suggested that $rbbp4^{\Delta 4/\Delta 4}$

241   mutant neural precursors undergo apoptosis before initiating differentiation. To examine

242   whether apoptosis was linked to the DNA damage response, wildtype and $rbbp4^{\Delta 4/\Delta 4}$ mutant

243   tissues were labeled with an antibody to γ-H2AX (Fig 4Q-4X), which recognizes phosphorylated

244   histone H2AX at DNA double strand breaks and more broadly labels damaged chromatin in

245   nuclei in apoptotic cells (27). Similar to activated Capsase-3, there is little γ-H2AX labeling in the

246   wildtype midbrain or retina at 2 dpf (Fig 4Q, 4S) or 3 dpf (Fig 4U), whereas there is a significant

247   increase of γ-H2AX positive cells in $rbbp4^{\Delta 4/\Delta 4}$ (Fig 4R, 4T, 4V-X). Close examination of γ-H2AX

248   labeling in the retina at 2 dpf revealed three distinct patterns in $rbbp4^{\Delta 4/\Delta 4}$ mutant cells. Some

249   cells contained nuclear foci typical of DNA double strand breaks (Fig 4T, dotted arrow), while

250   others had a defined nuclear ring (Fig 4L, open arrow) or pan-nuclear labeling (Fig 4T, closed

251   arrow) indicative of extensive genome wide DNA damage. Cells with γ-H2AX rings or pan-

252   nuclear labeling contained small fragmented nuclei characteristic of later stages of apoptosis

253   (Fig 4T). At 3dpf γ-H2AX labeling was restricted to the proliferative zones in the $rbbp4^{\Delta 4/\Delta 4}$

254   tectum and retina (Fig 4V). Together, the activated Caspase-3 and γ-H2AX labeling indicate

255   failure of $rbbp4^{\Delta 4/\Delta 4}$ mutant neural precursors to survive is due to persistent DNA damage and

256   activation of programmed cell death.

257

258

259   **Neural precursor apoptosis after Rbbp4 loss is dependent on Tp53**

260

261   To test whether apoptosis in $rbbp4^{\Delta 4/\Delta 4}$ neural precursors is activated by the Tp53-

262   dependent DNA damage response we knocked down Tp53 activity using an antisense

263   translation blocking $tp53$ morpholino (Fig 5A). Tp53 knock down did not affect development or

264   cell viability in the wildtype midbrain or retina at 2 dpf and 3 dpf, but was able to significantly

265   suppress activated Caspase-3 labeling and apoptosis in the $rbbp4^{\Delta 4/\Delta 4}$ midbrain and retina at 2

266   dpf (Fig 5B-5K). At 3 dpf,Tp53 knock down significantly reduced activated Caspase-3 labeling in

9

267   the *rbbp4*$^{\Delta 4/\Delta 4}$ retina but not the midbrain (Fig 5J and 5K), which may be due to a greater

268   decrease in midbrain proliferation compared to the retina. These results are consistent with

269   Rbbp4 preventing Tp53-dependent apoptosis in neural precursors. Tp53 knockdown was able

270   to suppress γ-H2AX labeling in the midbrain and retina of 2 dpf *rbbp4*$^{\Delta 4/\Delta 4}$ mutant embryos (Fig

271   5L-5O, 5T and 5U). By 3 dpf the suppressive effect was no longer significant (Fig 5P-5S, 5T and

272   5U), possibly due to reduced numbers of viable cells in the proliferative regions of the midbrain

273   and retina. Overall, the nearly complete suppression of activated Caspase-3 and γ-H2AX

274   labeling in 2 dpf *rbbp4*$^{\Delta 4/\Delta 4}$ mutant embryos after Tp53 knockdown together indicate Rbbp4 is

275   required to prevent persistent DNA damage and activation of Tp53 dependent programmed cell

276   death in neural precursors.

277

278

279   **Rbbp4 mutant retinal neural precursors fail to initiate quiescence and**

280   **differentiation**

281

282   The results presented above suggest loss of Rbbp4 may induce apoptosis in retinal

283   neural precursors that fail to become quiescent and initiate differentiation. We first used BrdU

284   labeling to follow the fate of *rbbp4*$^{\Delta 4/\Delta 4}$ mutant neural precursors in the post-embryonic retina.

285   Retinal neurogenesis proceeds in a conveyor belt pattern, with stem cells at the ciliary marginal

286   zone generating progenitors that become progressively more committed as they move inward in

287   the growing retina (28, 29). 2 dpf embryos were exposed to a 3-hour BrdU pulse and collected

288   immediately or chased until 3 dpf and 5 dpf. At the end of 2 dpf in wildtype retina BrdU

289   incorporates into stem cells at the CMZ and progenitors in the inner nuclear and newly

290   developing photoreceptor layers (Fig 6A). A similar pattern of BrdU incorporation was detected

291   in the *rbbp4*$^{\Delta 4/\Delta 4}$ mutant retina (Fig 6B). At 3 dpf BrdU labeled cells were found in the region

292   adjacent to the CMZ in both wildtype and *rbbp4*$^{\Delta 4/\Delta 4}$ (Fig 6C and 6D outline), however many

293   fewer BrdU positive cells were present in the mutant. By 5 dpf, BrdU positive cells were

294   incorporated into the ganglion and inner nuclear layers of the laminated region of the wildtype

295   retina (Fig 6E outline) but were missing from the *rbbp4*$^{\Delta 4/\Delta 4}$ mutant (Fig 6F). In the *rbbp4*$^{\Delta 4/\Delta 4}$

296   mutant, stem cells were still present but lacked BrdU label (Fig 6F arrow). BrdU labeled cells in

297   the central part of the *rbbp4*$^{\Delta 4/\Delta 4}$ mutant retina (Fig 6F) may represent rod photoreceptor

298   progenitors or early born Mueller glia in the inner nuclear layer. Together, these results suggest

299   neural progenitors or newborn neurons fail to survive in the absence of Rbbp4.

300

301   Neurogenesis in the zebrafish retina can be visualized by expression of genes in

302   discreet sectors that mark progressive steps in neural progenitor commitment (30). To identify

303   the stage at which $rbbp4^{\Delta 4/\Delta 4}$ neural precursors are lost we performed *in situ* hybridization on

304   3dpf wildtype and $rbbp4^{\Delta 4/\Delta 4}$ retina with probes to collage type XV alpha 1b (*mz98*) (31), cyclin

305   D1 (*ccnD1*) (32), atonal 7 (*ath5*) (33) and cyclin dependent kinase inhibitor 1Ca (*cdkn1c*) (34). In

306   wildtype, cells at the periphery of the ciliary marginal zone express stem cell marker *mz98* (Fig

307   6H arrow), followed by proliferating progenitors that express *ccnD1* (Fig 6I bracket), and then

308   *ath5*-expressing committed neural precursors (Fig 6J bracket). Lastly, *cdkn1c* expression marks

309   precursors arrested in G1 that will initiate quiescence and differentiation (Fig 6K arrow). In the

310    $rbbp4^{\Delta 4/\Delta 4}$ mutant retina *mz98*-expressing cells were present in the CMZ (Fig 6L arrow). The

311   population of *ccnd1*-labeled progenitors and *ath5*-expressing committed precursors was

312   significantly expanded in the mutant compared to wildtype (Fig 6M and 6N brackets). In

313   addition, *cdkn1c*-expression was not detected in the next adjacent sector (Fig 6O arrow). These

314   results indicate that in the absence of Rbbp4, *ath5*-expressing committed precursor loss occurs

315   before the transition when cells exit the cell cycle to initiate quiescence and differentiation.

316

317

318   **Rbbp4 is required for survival of *rb1*-mutant retinal neural precursors**

319

320   We previously demonstrated that in *rb1* mutant zebrafish larvae, neural progenitors can

321   re-enter the cell cycle, and phospho-Histone H3 labeled M-phase cells can be detected

322   throughout the *rb1* mutant brain and retina (11). To determine whether survival of *rb1* mutant

323   neural precursors is dependent on Rbbp4, we tested whether *rbbp4*; *rb1* double mutant neural

324   precursors undergo apoptosis (Fig 7A-7H, Fig S7). At 3dpf, in the $rbbp4^{\Delta 4/\Delta 4}$ mutant retina

325   activated caspase-3 and fragmented nuclei are observed in neural progenitors in the region

326   adjacent to the ciliary marginal zone (Fig 7F dashed outline). Activated caspase-3 labeling is

327   absent from $rb1^{\Delta 7/\Delta 7}$ mutant retina and brain, however, in the $rbbp4^{\Delta 4/\Delta 4}$; $rb1^{\Delta 7/\Delta 7}$ double mutant,

328   activated caspase-3 is present, similar to the single $rbbp4^{\Delta 4/\Delta 4}$ mutant (Fig 7G and 7H). Labeling

329   with phospho-Histone H3 antibodies confirm the $rb1^{\Delta 7/\Delta 7}$ single and $rbbp4^{\Delta 4/\Delta 4}$; $rb1^{\Delta 7/\Delta 7}$ double

330   mutants have increased numbers of cells in mitosis compared to wildtype brain and retina (Fig

331   7I-7P). These results show that loss of Rbbp4 can induce apoptosis in *rb1* mutant neural

332   precursors, indicating the viability of *rb1* mutant cells is dependent Rbbp4 (Fig 7Q).

333

334

Discussion

336

337   In this study we demonstrate *in vivo* Rbbp4 is essential for vertebrate neurogenesis and

338   is required for neural stem cell proliferation and neural precursor survival. While Rbbp4 was

339   originally identified as a binding partner of the Rb1 tumor suppressor, we show for the first time

340   that survival of *rb1*-mutant neural precursors is dependent on *rbbp4*. We find that Rbbp4 is

341   overexpressed in *rb1*-embryonal brain tumors and is upregulated across the spectrum of human

342   embryonal and glial tumor types. Together with recent studies examining the role of Rbbp4 in

343   glioblastoma DNA damage repair (9) and neuroblastoma tumor progression (10), our study

344   provides additional evidence that Rbbp4 might contribute to brain tumor cell survival by

345   promoting proliferation and circumventing DNA damage induced apoptosis.

346

347   Our analysis of zebrafish *rbbp4* mutants revealed Rbbp4 is necessary for neurogenesis

348   with distinct roles in neural stem and progenitor cells. Loss of Rbbp4 did not affect stem cell

349   survival, however, BrdU lineage tracing showed mutant stem cells underwent a limited number

350   of divisions before exiting the cell cycle. The morphology of the stem cells was abnormally

351   enlarged, which could represent the onset of senescence that is characterized by cellular

352   hypertrophy (35). These results are consistent with other *in vivo* and *in vitro* studies indicating a

353   role for Rbbp4 in preventing cellular senescence. Rbbp4 is a component of the DREAM/MuvB

354   complex that controls quiescence by promoting cell cycle gene expression and progression

355   through G2 (36), but has also been shown to be required for oncogene-induced senescence in

356   immortalized BJ fibroblasts (37). In Arabidopsis, the Rbbp4 homolog *AtMSI1* is necessary for

357   persistent growth of reproductive tissues through expression of homeotic genes and

358   heterochromatin assembly (38). In addition to controlling senescence through chromatin

359   structure and gene expression, Rbbp4 has been implicated in blocking cellular senescence

360   through the regulation of nuclear import (39). Lastly, cancer cells that maintain telomere length

361   using the alternative lengthening of telomere (ALT) pathway recruit NuRD to their telomeres

362   through the transcription factor ZNF827 (40). Recently it was shown that Rbbp4 binds ZNF827

363   (41), suggesting Rbbp4 might contribute to preventing cancer cell replicative senescence by

364   association of NuRD with telomeres. Together these studies suggest a critical role for Rbbp4 in

365   stem cell maintenance, possibly through multiple nuclear processes, including transcriptional

366   regulation of cell cycle progression, heterochromatin formation, telomere lengthening, and

367   nuclear transport.

12

368

369   A major finding in our study is the *in vivo* requirement for Rbbp4 to prevent Tp53-

370   dependent apoptosis in zebrafish neural progenitors in the growing midbrain and retina. In the

371   *rbbp4* mutant retina, the expansion of the *ath*5-positive progenitor population and the absence

372   of *cdkn1c*-expressing cells suggests progenitors fail to transition to a neural precursor and

373   initiate quiescence. The accumulation of γ-H2AX labeling in *rbbp4* mutant progenitors would

374   suggest persistent DNA damage activates the DNA damage response and Tp53-dependent

375   apoptosis. Given the role of Rbbp4 in multiple chromatin remodelers that regulate gene

376   expression, the primary effect of loss of Rbbp4 may be altered transcriptional regulation. This

377   could affect multiple pathways including the DNA damage response, as has been shown in

378   glioblastoma multiforme cells (9), leading to persistent DNA damage and activation of Tp53

379   apoptosis. Alternatively, loss of Rbbp4 could directly affect genome integrity in neural

380   precursors. Knockdown of Rbbp4 in cell culture leads to defects in DNA synthesis, nucleosome

381   assembly and heterochromatin formation (42, 43). Similar mechanisms may cause DNA

382   damage in zebrafish *rbbp4* mutant embryos, possibly through disruption of the CAF-1

383   nucleosome assembly factor that contains p150, p60, and Rbbp4 (44). In addition to the

384   classical γ-H2AX foci representing DNA double strand breaks (27), the majority of γ-H2AX

385   labeling in *rbbp4* mutant embryos appeared as pan-nuclear or nuclear rings, which mark

386   extensive DNA damage and disruption of chromatin integrity (45). γ-H2AX nuclear ring labeling

387   has been described in response to activation of death receptors by TRAIL ligand, indicating

388   extrinsic signaling independent of Tp53 could also contribute to apoptosis in *rbbp4* mutant cells

389   (46). However, our ability to suppress apoptosis after Tp53 knockdown in *rbbp4* mutant

390   embryos would argue that intrinsic activation of Tp53 and the DNA damage response is

391   responsible for apoptosis.

392

393   In conclusion, our study indicates Rbbp4 may promote proliferation and survival of

394   wildtype and *rb1* mutant neural precursors by circumventing DNA damage induced apoptosis.

395   Disruption of transcriptional regulation, chromatin assembly and DNA repair could each

396   contribute to apoptosis after loss of Rbbp4. Knockdown of Tp53 blocked apoptosis, providing a

397   means to prevent cell death and examine how loss of Rbbp4 changes the epigenetic landscape

398   and gene expression profile in *rbbp4* mutant neural precursors. These future studies would

399   provide new insight into the mechanism by which Rbbp4 and its associated chromatin

400   remodelers promote proliferation and survival during neurogenesis.

401

Materials and Methods

403

Zebrafish care and husbandry

405

406   Zebrafish were reared in an Aquatic Habitat system (Aquatic Ecosystems, Inc., Apopka,

407   FL). Fish were maintained on a 14-hr light/dark cycle at 27°C. Transgenic lines were established

408   in a WIK wild type strain obtained from the Zebrafish International Research Center

409   (http://zebrafish.org/zirc/home/guide.php). The zebrafish *rbbp4* and *rb1* alleles used in this study

410   were isolated by CRISPR-Cas9 or TALEN targeting and described previously: *rbbp4* 4 base pair

411   (bp) deletion allele *rbbp4Δ4^{is60}* (11); *rb1* 7bp deletion allele *rb1Δ7^{is54}* (18). For *in situ*

412   hybridization and immunohistochemistry experiments, embryos were collected and maintained

413   at 28.5°C in fish water (60.5 mg ocean salts/l) until harvesting. Embryos were staged according

414   to published guidelines (47). All experimental protocols were approved by the Iowa State

415   University Institutional Animal Care and Use Committee (Log # 11-06-6252-I) and are in

416   compliance with American Veterinary Medical Association and the National Institutes of Health

417   guidelines for the humane use of laboratory animals in research.

418

419

Larval genotyping and *tp53* morpholino injections

421

422   Primers to amplify *rbbp4* exon 2 containing the *rbbp4Δ4^{is60}* mutation: Forward 5′

423   GCGTGATGACAGATCTCATATTGTTTTCCC 3′; Reverse 5′ CTGGTGACATCTGGCAACCACT

424   3′. Primers to amplify *rb1* exon 2 containing the *rb1Δ7^{is54}* mutation: Forward 5'-

425   TTTCCAGACACAAGGACAAGGATCC-3'; Reverse 5'-

426   GCAGATATCAGAAGAAAGAGTACATTTGTCTT-3'. To inhibit Tp53-dependent apoptosis,

427   embryos were injected at the one cell stage with 2 ng of *tp53* translation blocking morpholino

428   GCGCCATTGCTTTGCAAGAATTG (48) (Gene Tools; ZDB-MRPHLNO-070126-7.

429

430

Isolation of transgenic line *Tg(Tol2<ubi:rbbp4-2AGFP>)^{is61}*

432

14

433   The *rbbp4* 1275 bp cDNA minus the translation termination codon was amplified by

434   reverse transcription PCR with Forward 5'-catgTCTAGATGTGGAGTCGTTATGGCTG-3' and

435   Reverse 5'-catgGGATCCTCCCTGAACCTCAGTGTCTG-3' primers that included 5' *Xba*I and 3'

436   *BamH*I sites, respectively. The *Tol2<ubi:rbbp4-2AGFP>* transgene was assembled using the

437   NEBuilder HiFi DNA Assembly protocol and mix (New England Biolabs E2621S) in the mini-

438   *pTol2* vector (49). The zebrafish *ubiquitin* promoter (50) was cloned into the vector followed by

439   the *rbbp4* cDNA, an in-frame 2A viral peptide GFP cassette (51) and the zebrafish β-*actin*

440   3'UTR (Dr. Darius Balciunas, Temple University; (52)). 1μg of linearized *pT3TS-Tol2*

441   transposase plasmid (49) was used as template for *in vitro* synthesis of *Tol2* transposase

442   capped, polyadenylated mRNA with T3 mMessage mMachine High Yield Capped RNA

443   transcription kit (Ambion AM1348). Synthesized mRNA was precipitated with LiCl and

444   resuspended in RNase, DNase-free molecular grade water. The *Tg(Tol2<ubi:rbbp4-2AGFP>)[is61]*

445   transgenic line was isolated by co-injection into 1-cell WIK zebrafish embryos of 25pg *Tol2*

446   vector plus 100pg *Tol2* mRNA. 14 founder fish were screened for germline transmission of

447   ubiquitously expressed GFP. A single F1 adult that showed Mendelian transmission of the

448   *Tol2<ubi:rbbp4-2AGFP>* transgene to the F2 generation was used to establish the line.

449

450

451   **Immunohistochemistry**

452

453   Embryonic (2 dpf) or larval (3-5 dpf) zebrafish were anesthetized in MS-222 Tricaine

454   Methanesulonate and head and trunk dissected. Trunk tissue was placed in 20μl 50mM NaOH

455   for genotyping. Heads were fixed in 4% paraformaldehyde overnight at 4°C, incubated in 30%

456   sucrose overnight at 4°C, then processed and embedded in Tissue-Tek OCT (Fisher 4583).

457   Processing and embedding of zebrafish wildtype adult brain and *rb1*-brain tumor tissue was as

458   described (18). Immunolabeling was performed on TALEN targeted *rb1*-brain tumors from three

459   fish; tumor tissue from two of these fish (individuals #7 and #10) was also used for RNA-Seq

460   libraries in our previous analysis of the *rb1*-embryonal brain tumor transcriptome (11). Tissues

461   were sectioned at 14-16 μm on a Microm HM 550 cryostat. For BrdU labeling experiments, 2 dpf

462   embryos were incubated in 5 μM BrdU (Sigma B5002) in embryo media (53) for 2.5 hours,

463   placed in fresh fish water, then sacrificed immediately or at 3 dpf and 5 dpf. To aid BrdU antigen

464   retrieval tissues were pretreated with 2 M HCl. For RBBP4 labeling, antigen retrieval was

465   performed by placing slides in boiling 10 mM NaCitrate and allowing the solution to cool to room

466   temperature. Antibodies used for labeling: rabbit polyclonal anti-RB Binding Protein 4 RBBP4

467 1:200 (Bethyl A301-206A-T, RRID: AB_890631); rabbit polyclonal anti-SOX2 1:200 (EMD

468 Millipore AB5603, RRID:AB_2286686); mouse monoclonal anti-proliferating cell nuclear antigen

469 PCNA 1:300 (Sigma P8825); mouse monoclonal anti-glial fibrillary acid protein GFAP 1:1000

470 (Zebrafish International Research Center zrf-1); rabbit polyclonal anti-phospho-Histone H3 PH3

471 1:1000 (Cell Signaling Technology; 9701); mouse monoclonal anti-phospho-Histone H3 (Ser10),

472 clone 3H10 1:500 (Millipore 05-806); rabbit polyclonal anti-Brain Lipid Binding Protein BLBP

473 1:200 (Abcam ab32423); mouse monoclonal anti-HuC/D 1:500 (Invitrogen A-21271); rabbit

474 polyclonal anti-gamma H2A histone family, member X γ-H2AX 1:200 (GeneTex GTX127342);

475 rabbit polyclonal anti-CASPASE-3 1:500 (BD Biosciences 559565); mouse monoclonal anti-SV2

476 1:100 (Developmental Studies Hybridoma Bank AB_2315387); rabbit polyclonal anti-

477 CALRETININ 1:1000 (Millipore AB5054); mouse monoclonal anti-BrdU 1:500 (Bio-Rad

478 MCA2483); Alexa-594 (Invitrogen A-11005) and Alexa-488 (Invitrogen A-11008) conjugated

479 secondary antibodies 1:500. Tissues were counterstained with 5 µg/ml DAPI and mounted in

480 Fluoro-Gel II containing DAPI (Electron Microscopy Sciences 17985-50) and imaged on a Zeiss

481 LSM700 laser scanning confocal.

482

483

484

485 *in situ* **hybridization and alcian blue staining**

486

487   cDNA was amplified by reverse transcription-polymerase chain reaction out of total RNA

488 isolated from wild-type 5 day post-fertilization embryos and cloned into the pCR4-TOPO vector

489 (Invitrogen). Primers for amplification: *mz98* forward 5′-CCGGACACTACACACTCAATGC-3′,

490 *mz98* reverse 5′-GTGCTGGATGTAGCTGTTCTCG-3′; *ccnD1* forward 5′-

491 GCGAAGTGGATACCATAAGAAGAGC-3′, *ccnD*1 reverse 5′-

492 GCTCTGATGTATAGGCAGTTTGG-3′; *ath5* forward 5′-GATTCCAGAGACCCGGAGAAG-3′,

493 *ath5* reverse 5′-CAGAGGCTTTCGTAGTGGTAGGAG-3′; *cdkn1c* forward 5′-

494 CGTGGACGTATCAAGCAATCTGG-3′, *cdkn1c* reverse 5′-GTCTGTAATTTGCGGCGTGC-3′.

495 Digoxigenin-labeled probes were synthesized using T3 RNA polymerase (Roche

496 #11031163001) and DIG RNA labeling mix (Roche #11277073910) according to the

497 manufacturer's instructions and stored in 50% formamide at −20°C. Embryonic and larval

498 zebrafish tissues were fixed in 4% paraformaldehyde and embedded in Tissue-Tek OCT (Fisher

499 4583). *in situ* hybridization was performed on 14–16 µm cryosections. For alcian blue staining of

500 cartilage, zebrafish larvae were anesthetized and fixed in 4% paraformaldehyde overnight at

16

501   4°C and incubated in 0.1% alcian blue solution overnight at 4°C. Embryos were rinsed in acidic

502   ethanol and stored in 70% glycerol. Whole larvae and tissue sections were imaged on a Zeiss

503   Discovery.V12 stereomicroscope or Zeiss Axioskop 2 microscope and photographed with a

504   Nikon Rebel camera.

505

506

507

508   **Western blotting**

509

510   Whole protein extract was generated by dounce homogenization of ~70 5 dpf embryos

511   in 200 uL Cell Extraction Buffer (ThermoFisher FNN0011). Lysates were run on a NuPAGE™

512   12% Bis-Tris Protein Gel (Invitrogen NP0342BOX) and blotted onto PVDF membrane (BioRAD

513   1620177). Membranes were incubated in either rabbit polyclonal anti-RB Binding Protein 4

514   RBBP4 (Bethyl A301-206A-T) at 1:800 or mouse monoclonal anti-β-actin (Sigma A2228) at

515   1:5000 overnight at 4°C, followed by Anti-Rabbit IgG F(ab′)2-Alkaline Phosphatase (Sigma

516   SAB3700833) or Anti-Mouse IgG F(ab′)2-Alkaline Phosphatase (Sigma SAB3700994) at 1:500

517   for one hour at room temperature. Membranes were developed with CSPD (Roche

518   11655884001) and imaged on a BioRAD Molecular Imager ChemiDoc XRS System.

519

520

521

522   **Quantification and Statistical Analysis**

523

524   Statistical analysis was performed using GraphPad Prism software. Data plots represent

525   mean $\pm$ s.d. p values were calculated with one-tailed Student's t-test. Statistical parameters are

526   included in the Figure legends.

527

528

529

530   **Acknowledgements**

531

534

535

Author Contributions

537

538   L.E.S. and M.M. conceived and designed the experiments and wrote the manuscript.

539   L.E.S., M.P.A. and W.A.W. built reagents, performed and documented experiments, and

540   analyzed results. M.K. performed human tumor expression analysis.

541

542

References

544   1.   Song JJ, Garlick JD, Kingston RE. Structural basis of histone H4 recognition by p55.
545   Genes Dev. 2008;22(10):1313-8.
546   2.   Nowak AJ, Alfieri C, Stirnimann CU, Rybin V, Baudin F, Ly-Hartig N, et al. Chromatin-
547   modifying complex component Nurf55/p55 associates with histones H3 and H4 and polycomb
548   repressive complex 2 subunit Su(z)12 through partially overlapping binding sites. J Biol Chem.
549   2011;286(26):23388-96.
550   3.   Moody RR, Lo MC, Meagher JL, Lin CC, Stevers NO, Tinsley SL, et al. Probing the
551   interaction between the histone methyltransferase/deacetylase subunit RBBP4/7 and the
552   transcription factor BCL11A in epigenetic complexes. J Biol Chem. 2017.
553   4.   Song R, Wang ZD, Schapira M. Disease Association and Druggability of WD40 Repeat
554   Proteins. J Proteome Res. 2017;16(10):3766-73.
555   5.   Torrado M, Low JKK, Silva APG, Schmidberger JW, Sana M, Sharifi Tabar M, et al.
556   Refinement of the subunit interaction network within the nucleosome remodelling and
557   deacetylase (NuRD) complex. FEBS J. 2017;284(24):4216-32.
558   6.   Lejon S, Thong SY, Murthy A, AlQarni S, Murzina NV, Blobel GA, et al. Insights into
559   association of the NuRD complex with FOG-1 from the crystal structure of an RbAp48.FOG-1
560   complex. J Biol Chem. 2011;286(2):1196-203.
561   7.   Alqarni SS, Murthy A, Zhang W, Przewloka MR, Silva AP, Watson AA, et al. Insight into
562   the architecture of the NuRD complex: structure of the RbAp48-MTA1 subcomplex. J Biol
563   Chem. 2014;289(32):21844-55.
564   8.   Zhang Q, Vo N, Goodman RH. Histone binding protein RbAp48 interacts with a complex
565   of CREB binding protein and phosphorylated CREB. Mol Cell Biol. 2000;20(14):4970-8.
566   9.   Kitange GJ, Mladek AC, Schroeder MA, Pokorny JC, Carlson BL, Zhang Y, et al.
567   Retinoblastoma Binding Protein 4 Modulates Temozolomide Sensitivity in Glioblastoma by
568   Regulating DNA Repair Proteins. Cell reports. 2016;14(11):2587-98.
569   10.   Li D, Song H, Mei H, Fang E, Wang X, Yang F, et al. Armadillo repeat containing 12
570   promotes neuroblastoma progression through interaction with retinoblastoma binding protein 4.
571   Nature communications. 2018;9(1):2829.
572   11.   Schultz LE, Haltom JA, Almeida MP, Wierson WA, Solin SL, Weiss TJ, et al. Epigenetic
573   regulators Rbbp4 and Hdac1 are overexpressed in a zebrafish model of RB1 embryonal brain
574   tumor, and are required for neural progenitor survival and proliferation. Dis Model Mech.
575   2018;11(6).
576   12.   Azzarelli R, Simons BD, Philpott A. The developmental origin of brain tumours: a cellular
577   and molecular framework. Development. 2018;145(10).

578   13.   Qian YW, Wang YC, Hollingsworth RE, Jones D, Ling N, Lee EY. A retinoblastoma-
579   binding protein related to a negative regulator of Ras in yeast. Nature. 1993;364(6438):648-52.
580   14.   Lu X, Horvitz HR. lin-35 and lin-53, two genes that antagonize a C. elegans Ras
581   pathway, encode proteins similar to Rb and its binding protein RbAp48. Cell. 1998;95(7):981-91.
582   15.   Litovchick L, Sadasivam S, Florens L, Zhu X, Swanson SK, Velmurugan S, et al.
583   Evolutionarily conserved multisubunit RBL2/p130 and E2F4 protein complex represses human
584   cell cycle-dependent genes in quiescence. Molecular cell. 2007;26(4):539-51.
585   16.   Ferguson KL, Slack RS. The Rb pathway in neurogenesis. Neuroreport. 2001;12(9):A55-
586   62.
587   17.   Fong BC, Slack RS. RB: An essential player in adult neurogenesis. Neurogenesis
588   (Austin). 2017;4(1):e1270382.
589   18.   Solin SL, Shive HR, Woolard KD, Essner JJ, McGrail M. Rapid tumor induction in
590   zebrafish by TALEN-mediated somatic inactivation of the retinoblastoma1 tumor suppressor
591   rb1. Scientific reports. 2015;5:13745.
592   19.   Gyda M, Wolman M, Lorent K, Granato M. The tumor suppressor gene retinoblastoma-1
593   is required for retinotectal development and visual function in zebrafish. PLoS Genet.
594   2012;8(11):e1003106.
595   20.   Johann PD, Erkek S, Zapatka M, Kerl K, Buchhalter I, Hovestadt V, et al. Atypical
596   Teratoid/Rhabdoid Tumors Are Comprised of Three Epigenetic Subgroups with Distinct
597   Enhancer Landscapes. Cancer Cell. 2016;29(3):379-93.
598   21.   Sturm D, Orr BA, Toprak UH, Hovestadt V, Jones DT, Capper D, et al. New Brain Tumor
599   Entities Emerge from Molecular Classification of CNS-PNETs. Cell. 2016;164(5):1060-72.
600   22.   Taylor MD, Northcott PA, Korshunov A, Remke M, Cho YJ, Clifford SC, et al. Molecular
601   subgroups of medulloblastoma: the current consensus. Acta neuropathologica.
602   2012;123(4):465-72.
603   23.   Mueller T, Wullimann MF. Anatomy of neurogenesis in the early zebrafish brain. Brain
604   Res Dev Brain Res. 2003;140(1):137-55.
605   24.   Stigloher C, Chapouton P, Adolf B, Bally-Cuif L. Identification of neural progenitor pools
606   by E(Spl) factors in the embryonic and adult brain. Brain Res Bull. 2008;75(2-4):266-73.
607   25.   Wullimann MF, Puelles L. Postembryonic neural proliferation in the zebrafish forebrain
608   and its relationship to prosomeric domains. Anat Embryol (Berl). 1999;199(4):329-48.
609   26.   Schmitt EA, Dowling JE. Early retinal development in the zebrafish, Danio rerio: light and
610   electron microscopic analyses. J Comp Neurol. 1999;404(4):515-36.
611   27.   Burma S, Chen BP, Murphy M, Kurimasa A, Chen DJ. ATM phosphorylates histone
612   H2AX in response to DNA double-strand breaks. J Biol Chem. 2001;276(45):42462-7.
613   28.   Cerveny KL, Varga M, Wilson SW. Continued growth and circuit building in the
614   anamniote visual system. Developmental neurobiology. 2012;72(3):328-45.
615   29.   Deves M, Bourrat F. Transcriptional mechanisms of developmental cell cycle arrest:
616   problems and models. Seminars in cell & developmental biology. 2012;23(3):290-7.
617   30.   Cerveny KL, Cavodeassi F, Turner KJ, de Jong-Curtain TA, Heath JK, Wilson SW. The
618   zebrafish flotte lotte mutant reveals that the local retinal environment promotes the
619   differentiation of proliferating precursors emerging from their stem cell niche. Development.
620   2010;137(13):2107-15.
621   31.   Pujic Z, Omori Y, Tsujikawa M, Thisse B, Thisse C, Malicki J. Reverse genetic analysis
622   of neurogenesis in the zebrafish retina. Dev Biol. 2006;293(2):330-47.
623   32.   Das G, Choi Y, Sicinski P, Levine EM. Cyclin D1 fine-tunes the neurogenic output of
624   embryonic retinal progenitor cells. Neural Dev. 2009;4:15.
625   33.   Masai I, Stemple DL, Okamoto H, Wilson SW. Midline signals regulate retinal
626   neurogenesis in zebrafish. Neuron. 2000;27(2):251-63.
627   34.   Shkumatava A, Neumann CJ. Shh directs cell-cycle exit by activating p57Kip2 in the
628   zebrafish retina. EMBO Rep. 2005;6(6):563-9.

629   35.   Demidenko ZN, Blagosklonny MV. Quantifying pharmacologic suppression of cellular
630   senescence: prevention of cellular hypertrophy versus preservation of proliferative potential.
631   Aging (Albany NY). 2009;1(12):1008-16.
632   36.   Sadasivam S, Duan S, DeCaprio JA. The MuvB complex sequentially recruits B-Myb
633   and FoxM1 to promote mitotic gene expression. Genes Dev. 2012;26(5):474-89.
634   37.   Litovchick L, Florens LA, Swanson SK, Washburn MP, DeCaprio JA. DYRK1A protein
635   kinase promotes quiescence and senescence through DREAM complex assembly. Genes Dev.
636   2011;25(8):801-13.
637   38.   Hennig L, Taranto P, Walser M, Schonrock N, Gruissem W. Arabidopsis MSI1 is
638   required for epigenetic maintenance of reproductive development. Development.
639   2003;130(12):2555-65.
640   39.   Tsujii A, Miyamoto Y, Moriyama T, Tsuchiya Y, Obuse C, Mizuguchi K, et al.
641   Retinoblastoma-binding Protein 4-regulated Classical Nuclear Transport Is Involved in Cellular
642   Senescence. J Biol Chem. 2015;290(49):29375-88.
643   40.   Conomos D, Reddel RR, Pickett HA. NuRD-ZNF827 recruitment to telomeres creates a
644   molecular scaffold for homologous recombination. Nature structural & molecular biology.
645   2014;21(9):760-70.
646   41.   Yang SF, Sun AA, Shi Y, Li F, Pickett HA. Structural and functional characterization of
647   the RBBP4-ZNF827 interaction and its role in NuRD recruitment to telomeres. The Biochemical
648   journal. 2018.
649   42.   Satrimafitrah P, Barman HK, Ahmad A, Nishitoh H, Nakayama T, Fukagawa T, et al.
650   RbAp48 is essential for viability of vertebrate cells and plays a role in chromosome stability.
651   Chromosome research : an international journal on the molecular, supramolecular and
652   evolutionary aspects of chromosome biology. 2016;24(2):161-73.
653   43.   Hayashi T, Fujita Y, Iwasaki O, Adachi Y, Takahashi K, Yanagida M. Mis16 and Mis18
654   are required for CENP-A loading and histone deacetylation at centromeres. Cell.
655   2004;118(6):715-29.
656   44.   Verreault A, Kaufman PD, Kobayashi R, Stillman B. Nucleosome assembly by a
657   complex of CAF-1 and acetylated histones H3/H4. Cell. 1996;87(1):95-104.
658   45.   Solier S, Pommier Y. The nuclear gamma-H2AX apoptotic ring: implications for cancers
659   and autoimmune diseases. Cell Mol Life Sci. 2014;71(12):2289-97.
660   46.   Wang S, El-Deiry WS. TRAIL and apoptosis induction by TNF-family death receptors.
661   Oncogene. 2003;22(53):8628-33.
662   47.   Kimmel CB, Ballard WW, Kimmel SR, Ullmann B, Schilling TF. Stages of embryonic
663   development of the zebrafish. Dev Dyn. 1995;203(3):253-310.
664   48.   Robu ME, Larson JD, Nasevicius A, Beiraghi S, Brenner C, Farber SA, et al. p53
665   activation by knockdown technologies. PLoS Genet. 2007;3(5):e78.
666   49.   Balciunas D, Wangensteen KJ, Wilber A, Bell J, Geurts A, Sivasubbu S, et al.
667   Harnessing a high cargo-capacity transposon for genetic applications in vertebrates. PLoS
668   Genet. 2006;2(11):e169.
669   50.   Mosimann C, Kaufman CK, Li P, Pugach EK, Tamplin OJ, Zon LI. Ubiquitous transgene
670   expression and Cre-based recombination driven by the ubiquitin promoter in zebrafish.
671   Development. 2011;138(1):169-77.
672   51.   Trichas G, Begbie J, Srinivas S. Use of the viral 2A peptide for bicistronic expression in
673   transgenic mice. BMC Biol. 2008;6:40.
674   52.   McGrail M, Hatler JM, Kuang X, Liao HK, Nannapaneni K, Watt KE, et al. Somatic
675   mutagenesis with a Sleeping Beauty transposon system leads to solid tumor formation in
676   zebrafish. PLoS One. 2011;6(4):e18826.
677   53.   Westerfield M. The zebrafish book: a guide for the laboratory use of zebrafish (Danio
678   rerio). 3rd ed: University of Oregon Press; 1995.

20

679

680

Figure Legends

682

Fig 1. Rbbp4 is localized in the nucleus in adult neural stem and progenitors and is upregulated in zebrafish *rb1* and human embryonal brain tumors. (A) Hematoxylin-labeled cross-section and diagram of adult zebrafish midbrain. Representative transverse cryosections (n=3 independent animals) through adult zebrafish midbrain (B-E) or *rb1*-embryonal brain tumor (F-I) labeled with antibodies to Rbbp4 (green), proliferation maker PCNA (red), and nuclear stain DAPI (blue). Rbbp4 is detected in the nuclei of cells lining the midbrain ventricle (C, D) and throughout the peri-granular zone (E), and is enriched in PCNA positive cells (D, arrow). Section through *rb1*-brain tumor shows expansion of the ventricular zone (F, G). The lesion is filled with Rbbp4 positive cells that frequently co-label with PCNA (H, I). Hy, hypothalamus; OT, optic tectum; PGZ, peri-granular zone; v, midbrain ventricle. Scale bars: A, E 400 μm; B, F 100 μm; D, G, H 40 μm; C 20 μm. See also Fig S1. (J) *RBBP4* expression in human embryonal tumors. ATRT, Atypical Teratoid/Rhabdoid Tumors: ATRT_TYR (n=25), ATRT_SHH (n=20), ATRT_MYC (n=17); MB, Medulloblastoma: MB_WNT (n=40), MB_SHH (n=112), MB_GRP3 (n=81), MB_GRP4 (n=135); EWS, Ewing Sarcoma (n=2); CNS EFT_*CIC,* CNS Ewing sarcoma family tumor with *CIC* alteration (n=4); CNS HGNET_*BCOR*, CNS high-grade neuroepithelial tumor with *BCOR* alteration (n=16); CNS HGNET_*MN1*, CNS high-grade neuroepithelial tumor with *MN1* alteration (n=7); CNS-NB-*FOXR2*, CNS neuroblastoma with *FOXR2* activation (n=10); EMTR, embryonal tumors with multilayered rosettes (n=18).

701

Fig 2. Rbbp4 is highly expressed in embryonic neuroblasts and shows variable levels in neural stem cells, precursors and neurons in the larval brain. Lateral and dorsal views of head region in zebrafish 2 dpf embryo (A, B) and 5 dpf larva (C-D) with midbrain optic tectum (OT, arrows) and retina (R) labeled. (E-P) Representative transverse cryosections (n=3) through 2 dpf and 5dpf wildtype zebrafish midbrain labeled with antibodies to Rbbp4 (green), proliferation maker PCNA (red), and nuclear stain DAPI (blue). (E) Diagram of location of stem cells lining the midbrain ventricle and at the ciliary marginal zone (CMZ) of the retina. (F-H) Boxes outline the ventricle at the top of the thalamus in the midbrain (G) and the retina ciliary marginal zone (H, bracket). See also Fig S1. (I) Diagram of 5 dpf midbrain showing location of stem cells (red) and progenitors (blue) at the ventricle in the dorsal optic tectum and ventral thalamus (Th). (J-L) 5 dpf wildtype zebrafish midbrain. Higher magnification view of the medial

21

713   tectal proliferative zone (K) and midbrain ventricle (L). (M) Diagram of 5 dpf retina showing

714   location of stem cells and retinal precursors at the ciliary marginal zone and the three nuclear

715   retinal layers. (N-P) 5 dpf retina. Higher magnification view of the ciliary marginal zone (O) and

716   central laminated layers of the retina (P). The highly proliferative, PCNA+ population of cells are

717   outlined; arrows indicate cells co-labeled with Rbbp4 and PCNA. Rbbp4 is enriched in a subset

718   of neurons in the midbrain and vitreal side of the retinal inner nuclear layer. See also Fig S2.

719   GCL, ganglion cell layer; INL, inner nuclear layer; ONL, outer nuclear layer. Scale bars: 100 μm

720   A, B, F, J, N; 200 μm C, D; 20 μm G, H; 10 μm K, L, O, P.

721

722   **Fig 3. Rbbp4 is required for zebrafish brain and neural crest development and persistent**

723   **neurogenesis in the midbrain optic tectum and retina.** (A-K) *rbbp4* cDNA rescue of

724   *rbbp4$^{\Delta4/\Delta4}$* homozygotes demonstrates requirement for Rbbp4 in brain and neural crest

725   development. (A) Lateral view of 5 dpf wildtype zebrafish indicating location of measurements

726   for head height (black arrow) and eye width (white arrow). (B) Lateral view of 5 dpf *rbbp4$^{\Delta4/\Delta4}$*

727   homozygote showing gross defects including microcephaly and microphthalmia. Lateral and

728   ventral views of 5 dpf wildtype (C, E) and *rbbp4$^{\Delta4/\Delta4}$* homozygous (D, F) larva stained with alcian

729   blue to reveal cartilage structures. (G) Schematic of *Tol2<ubi:rbbp4-2AGFP>* cDNA rescue

730   construct driving expression of *rbbp4-2AGFP* by the *ubiquitin* promoter. (H) 5 dpf transgenic

731   *Tg*(*Tol2<ubi:rbbp4-2AGFP>*) and (I) 5 dpf transgenic *rbbp4$^{\Delta4/\Delta4}$* ; *Tg*(*Tol2<ubi:rbbp4-2AGFP>*)

732   larva showing rescue of the *rbbp4$^{\Delta4/\Delta4}$* homozygous mutant phenotype. (J) *rbbp4$^{\Delta4/\Delta4}$*

733   homozygotes (n=6) have a significantly smaller head than wildtype (n=3, *p*=0.0015). Transgenic

734   GFP+ *rbbp4$^{\Delta4/\Delta4}$* homozygotes (n=4) show no significant difference in head height compared to

735   GFP+ +/+ wildtype (n=4) (*p*=0.4595). (K) *rbbp4$^{\Delta4/\Delta4}$* homozygotes (n=8) have a significantly

736   smaller eye than wildtype (n=5, *p*=0.0001). Transgenic *rbbp4$^{\Delta4/\Delta4}$* GFP+ (n=5) show no

737   significant difference in eye size compared to GFP+ +/+ wildtype (n=8, *p*=0.6293). Data

738   represent mean ± s.d. *p* values calculated with one-tailed Student's *t*-test. ch, ceratohyal

739   cartilage; m, Meckel's cartilage; cbs, ceratobranchial cartilage. See also Fig S2 and Table S1.

740   (L-S) Transverse sections of midbrain and retina from wild type +/+ (n=5) and homozygous

741   mutant *rbbp4$^{\Delta4/\Delta4}$* (n=4) 5 dpf zebrafish larvae labeled with antibodies to proliferative marker

742   PCNA (red) and stem/progenitor marker Sox2 (green) and nuclear stain DAPI (blue). (L, N) In

743   wildtype PCNA and Sox2-positive stem cells line the midbrain ventricle (L, N dashed outline).

744   Sox2-positive progenitors lie adjacent to the ventricle in the tectum (N bracket). (N, O) PCNA

745   and Sox2-positive cells with enlarged morphology line the midbrain ventricles in *rbbp4$^{\Delta4/\Delta4}$*

746   mutant (O outline). The dorsal tectum is significantly reduced in height in the *rbbp4$^{\Delta4/\Delta4}$* mutant

747   (O bracket). (P, R) In wild type retina PCNA-positive stem cells are restricted to the outer edge

748   of the ciliary marginal zone (R outline). Sox2-positive amacrine and displaced amacrine cells

749   are distributed throughout the inner nuclear and ganglion cell layers. (Q, S) PCNA-positive stem

750   cells with enlarged, hypertrophic morphology at the ciliary marginal zone in $rbbp4^{\Delta4/\Delta4}$ mutant

751   retina (S outline). Arrow shows missing tissue adjacent to the ciliary marginal zone. Sox2-

752   positive cells representing early born amacrine cells are present in the retinal layers. See also

753   Fig S3. Scale bars: A-F 100 µm; 50 µm L, M, P, Q; 20 µm N, O, R, S.

754

755   **Fig 4. Accumulation of DNA damage and apoptosis in neural precursors underlies**

756   **defects in $rbbp4^{\Delta4/\Delta4}$ midbrain and retina neurogenesis.** See also Fig S3. Lateral (A-D) and

757   dorsal (E-H) images of 2 dpf and 3 dpf larva show the size of the optic tectum (arrows, OT) and

758   midbrain overall (brackets) is reduced in $rbbp4^{\Delta4/\Delta4}$ mutants compared to +/+ wildtype. (I-N)

759   Transverse sections of zebrafish midbrain and retina labeled with antibodies to the apoptosis

760   marker activated-Caspase-3 (green), neural marker HuC/D (red), and nuclear label DAPI (blue).

761   (I, K, M) Few activated Caspase-3 labeled cells are detected in wildtype at 2dpf (n=4) and 3 dpf

762   (n=3). (J, L, N) Extensive activated Caspase-3 labeling is present throughout the midbrain

763   tectum and retina in the $rbbp4^{\Delta4/\Delta4}$ mutant at 2 dpf (n=7) and 3 dpf (n=5). (L) Higher

764   magnification view of nuclear morphology shows pyknosis and nuclear fragmentation in the

765    $rbbp4^{\Delta4/\Delta4}$ mutant 2 dpf retina. (O, P) Counts of activated Caspase-3 positive cells plotted for

766   individual larva show a significant difference between wildtype and $rbbp4^{\Delta4/\Delta4}$ mutant at 2 dpf in

767   the midbrain (O, p=0.0022) and in the retina (P, p=0.0010). At 3 dpf the difference is no longer

768   significant in the midbrain (O, p=0.2569) and only slightly significant in the retina (P, p=0.0358),

769   due to loss of cells by apoptosis. (Q-V) Transverse sections of zebrafish midbrain and retina

770   labeled with an antibody to the DNA damage marker γ-H2AX (green) and nuclear label DAPI

771   (blue). (Q, S, U) Few γ-H2AX labeled cells are present in wildtype midbrain or retina at 2 dpf

772   (n=3) and 3 dpf (n=3). (R, T, V) In the $rbbp4^{\Delta4/\Delta4}$ mutants (n=3) at 2 dpf a significantly greater

773   number of cells with γ-H2AX labeling was present in the brain (W, p=0.0008) and retina (X,

774   p=0.0032). By 3 dpf (n=3) the number was not significantly different than in wildtype (midbrain

775   W, p=0.1211; retina X, p=0.0537), likely due to loss of cells by apoptosis. (T) Higher

776   magnification view of nuclear morphology and γ-H2AX labeling in the $rbbp4^{\Delta4/\Delta4}$ mutant 2dpf

777   retina. Closed arrow shows pannuclear staining; open arrow shows nuclear ring staining; dotted

778   arrow shows foci pattern of staining. Data represent mean ± s.d. p values calculated with one-

779   tailed Student's t-test. Scale bars: 100 µm (I, J, M, N, Q, R, U, V); 10 µm (K, L, S, T).

780

Fig 5. Tp53-dependent activation of DNA damage response and apoptosis in _rbbp4$^{\Delta4/\Delta4}$_
mutant neural precursors. 2 dpf and 3 dpf wildtype and _rbbp4$^{\Delta4/\Delta4}$_ larval midbrain sections
after _tp53_ knockdown. (A) Inhibition of Tp53 activity by antisense morpholino injection into
embryos from _rbbp4$^{\Delta4}$/+_ adult incross. (B-I) Activated Caspase-3 (green), HuC/D (red) and
DAPI (blue) labeling at 2 dpf (B-E) and 3 dpf (F-I). (J) Comparison of Caspase-3 positive cells in
the midbrain between un-injected and _tp53_ MO injected wildtype at 2 dpf (un-injected n=4; _tp53_
MO injected n=4; _p_=0.017), _rbbp4$^{\Delta4/\Delta4}$_ at 2 dpf (un-injected n=2; _tp53_ MO injected n=4;
_p_=0.0112), wildtype at 3 dpf (un-injected n=3; _tp53_ MO injected n=3; _p_=0.3349), and _rbbp4$^{\Delta4/\Delta4}$_
at 3 dpf (un-injected n=4; _tp53_ MO injected n=6; _p_=0.1736). (K) Comparison of Caspase-3
positive cells in the retina between un-injected and _tp53_ MO injected wildtype at 2 dpf (un-
injected n=4; _tp53_ MO injected n=4; _p_=0), _rbbp4$^{\Delta4/\Delta4}$_ at 2 dpf (un-injected n=2; _tp53_ MO injected
n=4; _p_=0.0032), wildtype at 3 dpf (un-injected n=3; _tp53_ MO injected n=3; _p_=0.0285), and
rbbp4$^{\Delta4/\Delta4}$ at 3 dpf (un-injected n=4; _tp53_ MO injected n=6; _p_=0.0037). (L-S) γ-H2AX labeling
(green), and nuclear stain DAPI (blue) at 2 dpf (K-N) and 3 dpf (O-R). (T) Comparison of γ-
H2AX positive cells in the midbrain between un-injected and _tp53_ MO injected wildtype at 2 dpf
(un-injected n=4; _tp53_ MO injected n=3; _p_=0.2344), _rbbp4$^{\Delta4/\Delta4}$_ at 2 dpf (un-injected n=2; _tp53_
MO injected n=4; _p_=0.0024), wildtype at 3 dpf (un-injected n=3; _tp53_ MO injected n=5;
_p_=0.1101), and _rbbp4$^{\Delta4/\Delta4}$_ at 3 dpf (un-injected n=6; _tp53_ MO injected n=10; _p_=0.0657). (U)
Comparison of γ-H2AX positive cells in the retina between un-injected and _tp53_ MO injected
wildtype at 2 dpf (un-injected n=4; _tp53_ MO injected n=3; _p_-value=0), _rbbp4$^{\Delta4/\Delta4}$_ at 2 dpf (un-
injected n=2; _tp53_ MO injected n=4; _p_=0.0001), wildtype at 3 dpf (un-injected n=3; _tp53_ MO
injected n=5; _p_=0.5784), and _rbbp4$^{\Delta4/\Delta4}$_ at 3 dpf (un-injected n=6; _tp53_ MO injected n=10;
_p_=0.0128). Data represent mean ± s.d. _p_ values calculated with one-tailed Student's _t_-test.
Scale bars: 100 µm.

Fig 6. Neural precursors fail to survive and initiate quiescence and differentiation in the
rbbp4$^{\Delta4/\Delta4}$ homozygous mutant retina. (A-F) BrdU pulse-chase labeling to examine the fate of
new born neurons in the _rbbp4$^{\Delta4/\Delta4}$_ mutant retina. (A, B) 2 dpf zebrafish embryos treated with a
2.5 hour BrdU pulse and immediately sacrificed. Transverse sections of retina from wildtype
(n=4) and _rbbp4$^{\Delta4/\Delta4}$_ mutants (n=5) were labeled with antibodies to BrdU and mitotic marker
phospho-Histone H3 (pH3). BrdU labels proliferating cells at the retina ciliary marginal zone and
cells scattered throughout the laminating retina. (C,D) Pulse-chased larvae at 3dpf. In wildtype
retina (n=8) BrdU labeled cells are located in the region adjacent to the cmz where neural
precursors and newly differentiated neurons reside (C outline). A small section of BrdU labeled

815   cells remains at the ciliary marginal zone in the *rbbp4$^{Δ4/Δ4}$* mutant retina (n=6) (D outline). (E,F)

816   Pulse-chased larvae at 5 dpf. In wildtype (n=7) the BrdU labeled cells are now more centrally

817   located in an older region of the growing retina (E outline). *rbbp4$^{Δ4/Δ4}$* mutant retina (n=7) older

818   born neurons in the central retina maintain BrdU labeling, however, BrdU-labeled newborn

819   neurons are absent. BrdU-negative stem cells persist at the ciliary marginal zone in the

820   *rbbp4$^{Δ4/Δ4}$* mutant (F arrow). (G) Diagram of pattern of gene expression marking stages of

821   neurogenesis in the developing zebrafish retina. (H-O) Transverse sections of 3 dpf zebrafish

822   retina labeled by *in situ* hybridization to examine expression of the stem cell marker *mz98* (H, L

823   arrows), proliferating progenitor marker *ccnD1* (I, M brackets), committed progenitor marker

824   *ath5* (J, N brackets) and differentiating precursor marker *cdkn1c* (K, O arrows). (H-K) Wildtype

825   retina (n=5) shows location of progressively committed precursor cell populations. (L-O) In the

826   *rbbp4$^{Δ4/Δ4}$* homozygous mutant retina (n=3) the proliferating and committed neural progenitor

827   cell populations are expanded compared to wild type. *cdkn1c* expression is absent in the

828   *rbbp4$^{Δ4/Δ4}$* mutant retina (O arrow). Scale bars: 50 µm.

829

830   **Fig 7. Rbbp4 is required for survival of *rb1/rb1* mutant retinal neural precursors**. 3 dpf wild

831   type +/+ (n=3), *rbbp4$^{Δ4/Δ4}$* (n=3), *rb1$^{Δ7/Δ7}$* (n=4), and *rbbp4$^{Δ4/Δ4}$; rb1$^{Δ7/Δ7}$* (n=2) siblings from a

832   *rbbp4$^{Δ4/+}$; rb1$^{Δ7/+}$* incross were sectioned and labeled with antibodies to activated caspase-3 and

833   HuC/D (A-H) or γ-H2AX and phospho-Histone H3 (I-P). Activated caspase-3 and nuclear

834   fragmentation are present in the region containing neural precursors (dashed outline) adjacent

835   to the ciliary marginal zone in both *rbbp4$^{Δ4/Δ4}$* and *rbbp4$^{Δ4/Δ4}$; rb1$^{Δ7/Δ7}$* mutants. (Q) Diagram

836   modeling requirement for Rbbp4 and Rb1 in retinal neurogenesis. Newborn retinal neural

837   precursors adjacent to the ciliary marginal zone will differentiate into neural cell types that

838   populate the retina ganglion cell, inner nuclear, and outer nuclear layers. Both Rbbp4 and Rb1

839   are required for neural precursors to initiate quiescence and differentiation, however, loss of

840   *rbbp4* leads to DNA damage-induced apoptosis, while loss of *rb1* allows entry into mitosis.

841   Double mutant precursors undergo apoptosis, indicating *rb1* mutant precursor viability is

842   dependent on Rbbp4. CMZ ciliary marginal zone; GCL ganglion cell layer; INL inner nuclear

843   layer; ONL outer nuclear layer. Scale bars: A-D, I-L 100 µm; E-H, M-P 20 µm.

844

845

846

847

848

849 **Supporting Information**

850

851 **S1 Fig. Related to Figs 1 and 2. (A-C) Rbbp4 protein is absent in *rbbp4Δ4/Δ4* homozygous**

852 **mutant larvae at 5 dpf. (D) *RBBP4* is highly expressed in many human brain tumor**

853 **entities.** (A) Western blot of whole protein lysate from wildtype +/+ and homozygous mutant

854 *rbbp4Δ4/Δ4* 5 dpf larvae probed with a rabbit polyclonal anti-Rbbp4 antibody. The antibody

855 recognizes a single polypeptide band of ~50kDA, close to the Rbbp4 predicted size of 48kDa.

856 The band is absent from the *rbbp4Δ4/Δ4* mutant protein extract. Lower panel, loading control

857 blot probed with mouse monoclonal antibody β-actin. (B, C) Rbbp4 and proliferative marker

858 PCNA antibody labeling of transverse sections through the head of 5 dpf wildtype (B) and

859 *rbbp4Δ4/Δ4* homozygous mutant (C) zebrafish larvae. Confocal images for each larva were

860 captured at approximately the same gain settings, with a slightly higher gain setting for the

861 homozygote, to confirm the absence of Rbbp4 signal. In wildtype brain (B) high levels of Rbbp4

862 are present in the nucleus of neurons in the tectum and thalamic regions, but are nearly absent

863 in the *rbbp4Δ4/Δ4* homozygote (C). Scale bars: 50 μm. (D) *RBBP4* Affymetrix data from 2284

864 human tumor samples (German Cancer Research Center DKFZ). atrt atypical teratoid/rhabdoid

865 tumor, cns central nervous system; cpc choroid plexus carcinoma; cph , cpp choroid plexus

866 papilloma; dipg diffuse intrinsic pontine glioma; etmr embryonal tumor with multilayered

867 rosettes; ews Ewing's sarcoma; mb medulloblastoma; ptpr papillary tumor of the pineal.

868

869

870 **S2 Fig. Related to Fig 2. Rbbp4 is ubiquitously expressed in neuroblasts in the**

871 **embryonic zebrafish brain and retina.** (A-A''') Representative transverse cryosections (n=3)

872 through 2 dpf wildtype zebrafish midbrain labeled with antibodies to Rbbp4 (green), proliferation

873 maker PCNA (red), and nuclear stain DAPI (blue). Boxes outline the ventricle at the top of the

874 thalamus in the midbrain (B) and the ciliary marginal zone (CMZ) of the retina (C). (B-B''')

875 Higher magnification view of the midbrain ventricle at the thalamus. (C-C''') Higher magnification

876 view of the ciliary marginal zone of the retina (C-C'''). Scale bars: 100 μm A-A'''; 20 μm B-C'''.

877

878

879 **S3 Fig. Related to Fig 2. Rbbp4 levels vary in neural stem cells, precursors and neurons**

880 **in the larval zebrafish brain and retina.** Representative transverse cryosections (n=3) of 5 dpf

881 wildtype zebrafish midbrain (A-A''') and retina (D-D''') labeled with antibodies to Rbbp4 (green),

882 proliferation maker PCNA (red), nuclear stain DAPI (blue). Higher magnification view of the

26

883   medial tectal proliferative zone (B-B'''), brain ventricle (C-C'''), ciliary marginal zone (E-E'''), and

884   central laminated layers of the retina (F-F'''). The highly proliferative, PCNA+ population of cells

885   are outlined; arrows indicate cells co-labeled with Rbbp4 and PCNA. Rbbp4 is enriched in a

886   subset of neurons in the midbrain and vitreal side of the retinal inner nuclear layer. GCL,

887   ganglion cell layer; INL, inner nuclear layer; ONL, outer nuclear layer. Scale bars: 100 μm A-A''',

888   D-D'''; 10 μm B-B''', C-C''', E-E''', F-F'''.

889

890

891   **S4 Fig. Related to Fig 3. Genotype confirmation of progeny from *rbbp4Δ4/Δ4*;**

892   ***Tg(Tol2<ubi:rbbp4-2AGFP>) rescue experiment.*** A 196 bp PCR amplicon surrounding *rbbp4*

893   exon 2 containing the 4 bp deletion mutation that overlaps a *Sml*I restriction enzyme site.

894   (Lanes 1, 2, 5, 6) *Sml*I digestion of +/+ wildtype larva (Fig 3A) and transgenic +/+ larva (Fig 3H)

895   generates 150 and 46 bp fragments. (Lanes 3, 4) In homozygous *rbbp4Δ4/Δ4* larvae (Fig 3B)

896   the *rbbp4Δ4* allele is resistant to digestion. (Lanes 7, 8) The resistant band in lane 8 confirms

897   the *Tg(Tol2<ubi:rbbp4-2AGFP>)* rescued larva (Fig 3I) is homozygous for the *rbbp4Δ4* allele. U,

898   un-digested; D, SmlI digested.

899

900

901   **S5 Fig. Related to Fig 3. Maternal Rbbp4 allows early born neurons and glia in**

902   ***rbbp4Δ4/Δ4* homozygotes to undergo normal neurogenesis and differentiation.**

903   Transverse section of midbrain and retina from wild type +/+ (n=3) and *rbbp4Δ4/Δ4*

904   homozygous (n=3) 5 dpf larva labeled with antibodies to glial markers Gfap (red) and Blbp

905   (green) and nuclear stain DAPI (blue). (A, C) In wild type midbrain Blbp and Gfap label radial

906   glia cell bodies and projections in the tectum (C bracket) and thalamic regions, respectively. (B,

907   D) The *rbbp4Δ4/Δ4* mutant midbrain contains mature radial glia in the thalamic region (B).

908   Intense Blbp labeling is present where hypertrophic stem cells are located at the ventricle (D

909   bracket). (E, G) Blbp and Gfap label Mueller glia cells bodies and projections across the inner

910   plexiform layer of the wild type retina. (F, H) Blbp and Gfap label persists in early born glia in the

911   *rbbp4Δ4/Δ4* mutant retina. (I-P) Transverse section of midbrain and retina from wild type +/+

912   (n=3) and *rbbp4Δ4/Δ4* mutant (n=3) 5 dpf larvae labeled with antibodies to the synaptic vesicle

913   marker Sv2 (red) and interneuron and ganglion cell marker Calretinin (green) and nuclear stain

914   DAPI (blue). (I, K) In wildtype brain, Sv2 labels the neuropil, and Calretinin labels the cell bodies

915   of a subset of mature neurons in the thalamus and tectum (K bracket). (J, L) The *rbbp4Δ4/Δ4*

916   mutant shows a reduction in the tectal neuropil and number of Calretinin-positive neurons (L

917 bracket). (M, O) Sv2 and Calretinin labeling in wild type retina. (N, P) Early born neurons

918 maintain Calretinin labeling and Sv2 labeled projections across the inner and outer plexiform

919 layers in the *rbbp4Δ4/Δ4* mutant retina. Scale bars: 50 µm A, B, E, F, I, J, M, N; 20 µm C, D, G,

920 H, K, L, O, P.

921

922

923 **S6 Fig. Related to Fig 4. Caspase-3 labeled rbbp4Δ4/Δ4 mutant retinal cells undergoing**

924 **apoptosis do not express the neuronal marker HuC/D.** (A-H) Transverse sections of 3 dpf

925 zebrafish retinas labeled with antibodies to the apoptosis marker activated Caspase-3 (green),

926 neuronal marker HuC/D (red), and nuclear stain DAPI (blue). (A-D) In wildtype +/+ HuC/D is

927 detected in neuron cell bodies in the inner nuclear layer and photoreceptor layer of the retina.

928 (E-H) In the *rbbp4Δ4/Δ4* homozygous retina cells expressing activated Caspase-3 do not co-

929 label with HuC/D. Arrow points to an activated Caspase-3-negative/HuC/D-positive cell

930 surrounded by activated Caspase-3-positive/HuC/D-negative cells. Scale bars: 100 µm.

931

932

933 **S7 Fig. Related to Fig 7. PCR genotyping to confirm genotype of +/+ wildtype, *rbbp4Δ4/Δ4***

934 **mutant, *rb1Δ7/Δ7* mutant, and *rbbp4Δ4/Δ4 ; rb1Δ7/Δ7* double mutant 3 dpf larvae from**

935 ***rbbp4Δ4/+ ; rb1Δ7/+* double heterozygous incross.** Each lane corresponds to an individual

936 progeny. A Gels of rbbp4 exon 2 PCR amplicons digested with *Sml*I. The digestion-resistant

937 bands correspond to the *rbbp4Δ4* allele. B Gels of rb1 exon 2 PCR amplicons. The 7bp deletion

938 and wildtype alleles can be distinguished based on band size.

939

940

941 **S1 Table. Related to Fig 3. Frequency of progeny genotypes and phenotypes from**

942 **heterozygous *rbbpΔ4/+* crossed to heterozygous *rbbpΔ4/+;Tg(Tol2<ubi:rbbp4-2AGFP>)***

943 **zebrafish.** Three independent crosses were set up between female *rbbpΔ4/+* heterozygotes

944 and male *rbbpΔ4/+;Tg(Tol2<ubi:rbbp4-2AGFP>)* transgenic heterozygotes. Embryo clutches

945 were sorted into positive and negative GFP groups at 2dpf. At 5dpf larvae were sorted by

946 phenotype and then genotyped. "Total" column shows approximately 50% GFP- and GFP+ in

947 each clutch, indicating the *Tg(Tol2<ubi:rbbp4-2AGFP>)* line contains a single transgene

948 integration. Scoring of GFP negative embryos revealed close to Mendelian segregation of the

949 *rbbpΔ4/Δ4* gross mutant phenotype in one quarter of the progeny (28.2%, 21.3%, 29%). A

950 random sampling of embryos from clutches 2 and 3 were genotyped and confirmed Mendelian

28

951   segregation of the phenotype with the *rbbpΔ4* allele. In each clutch, none of the GFP positive

952   embryos showed the rbbp4 mutant phenotype. Random sampling and genotyping confirmed ~

953   one quarter of morphologically normal GFP+ larvae were homozygous mutant *rbbpΔ4/Δ4*

954   (32.4%, 20.8%, 20.8%).

955

956

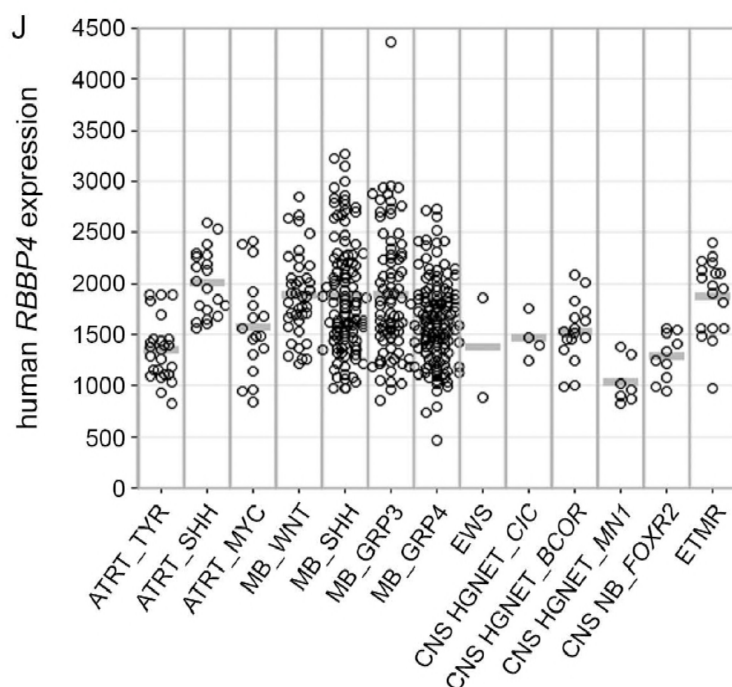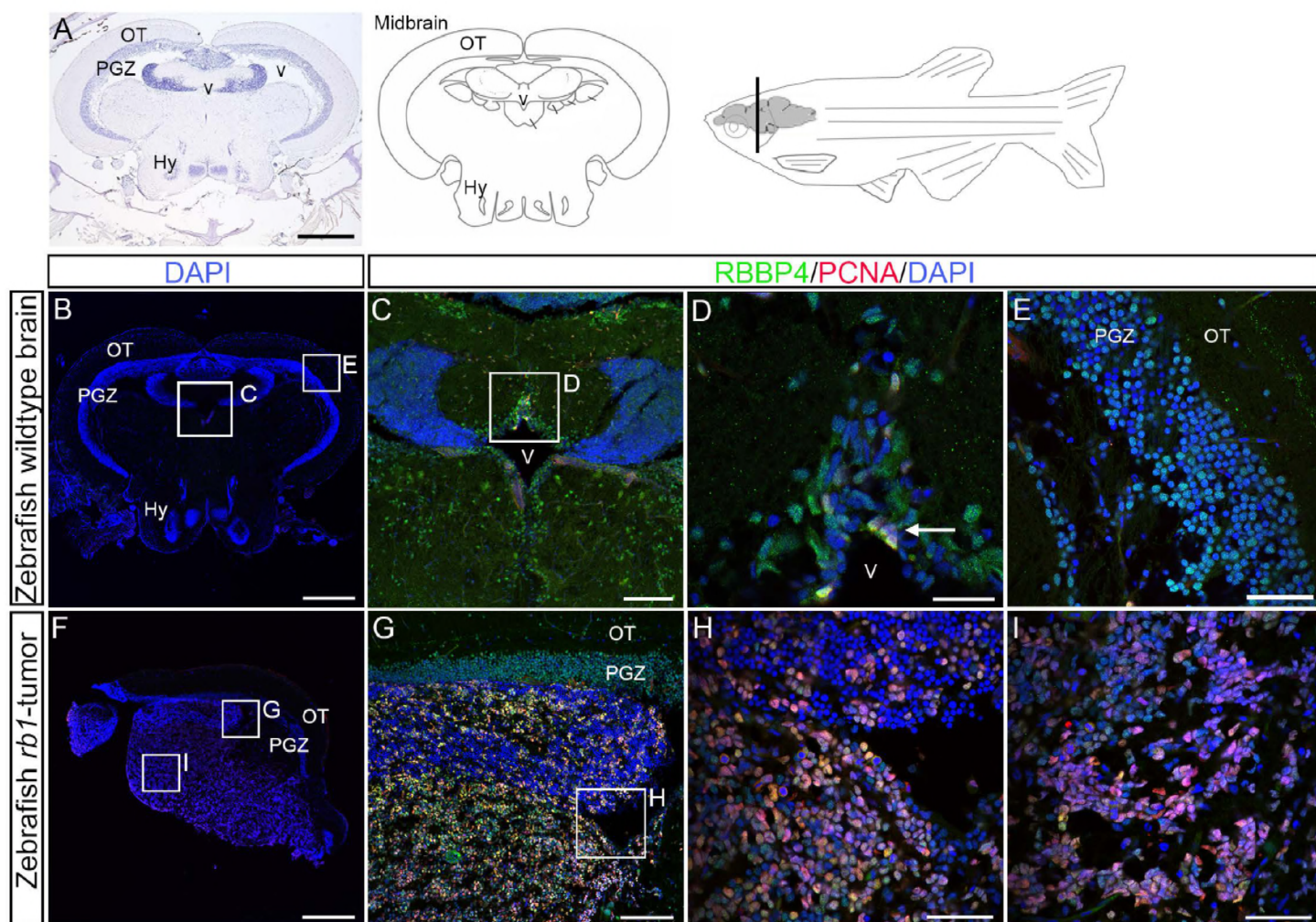957   **S2 Table. Sequences of primers used in this study.**

Fig 1. Rbbp4 is localized in the nucleus in zebrafish adult neural stem and progenitors, and is upregulated in zebrafish *rb1* and human embryonal brain tumors.

Fig 2. Rbbp4 is highly expressed in zebrafish embryonic neuroblasts and shows variable levels in neural stem cells, precursors and neurons in the larval brain.
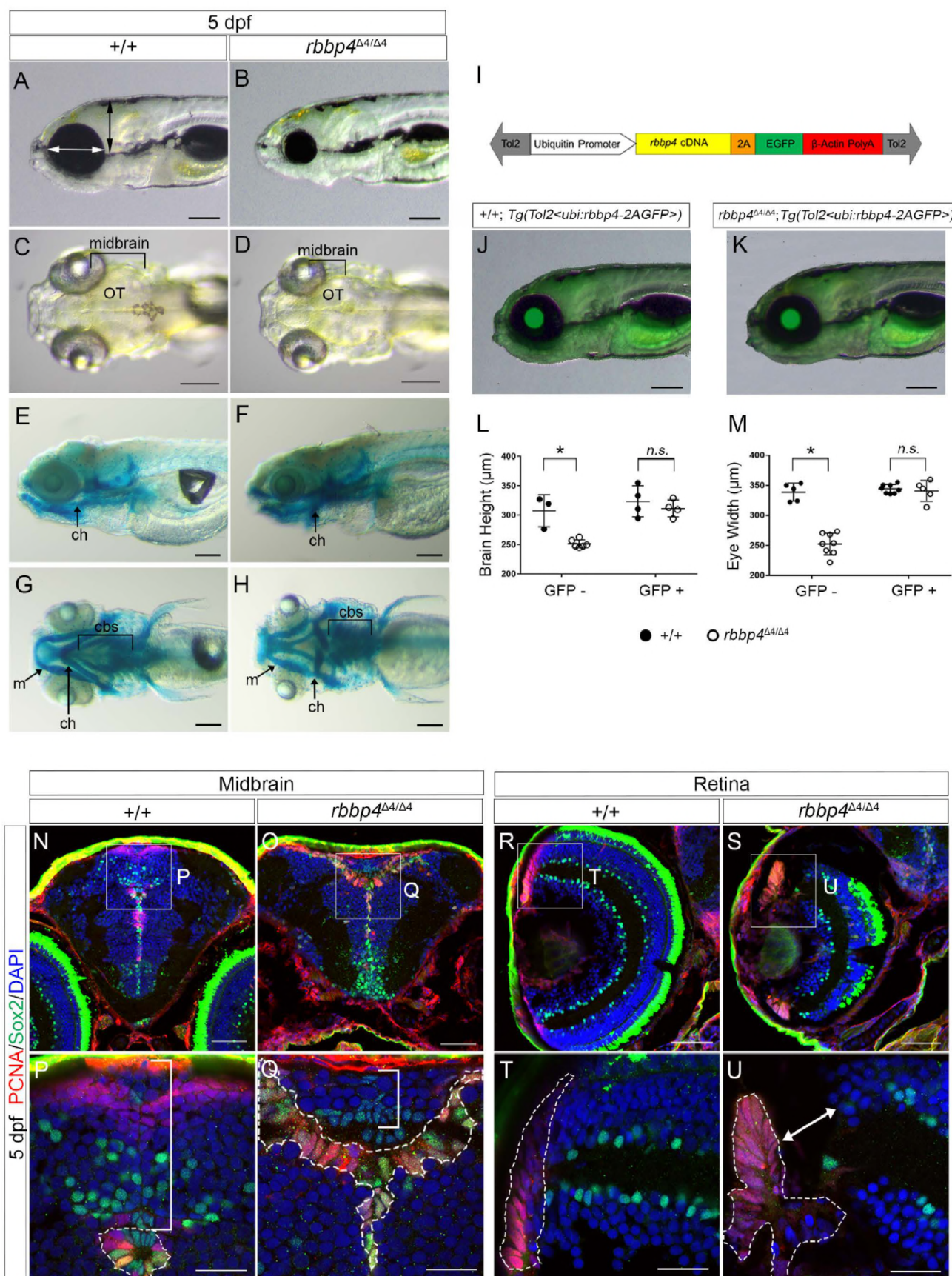
Fig 3. Rbbp4 is required for zebrafish brain and neural crest development and persistent neurogensis in the midbrain optic tectum and retina.

Fig 4. Accumulation of DNA damage and apoptosis in neural precursors underlies defects in *rbbp4*^{Δ4/Δ4} midbrain and retinal neurogenesis.
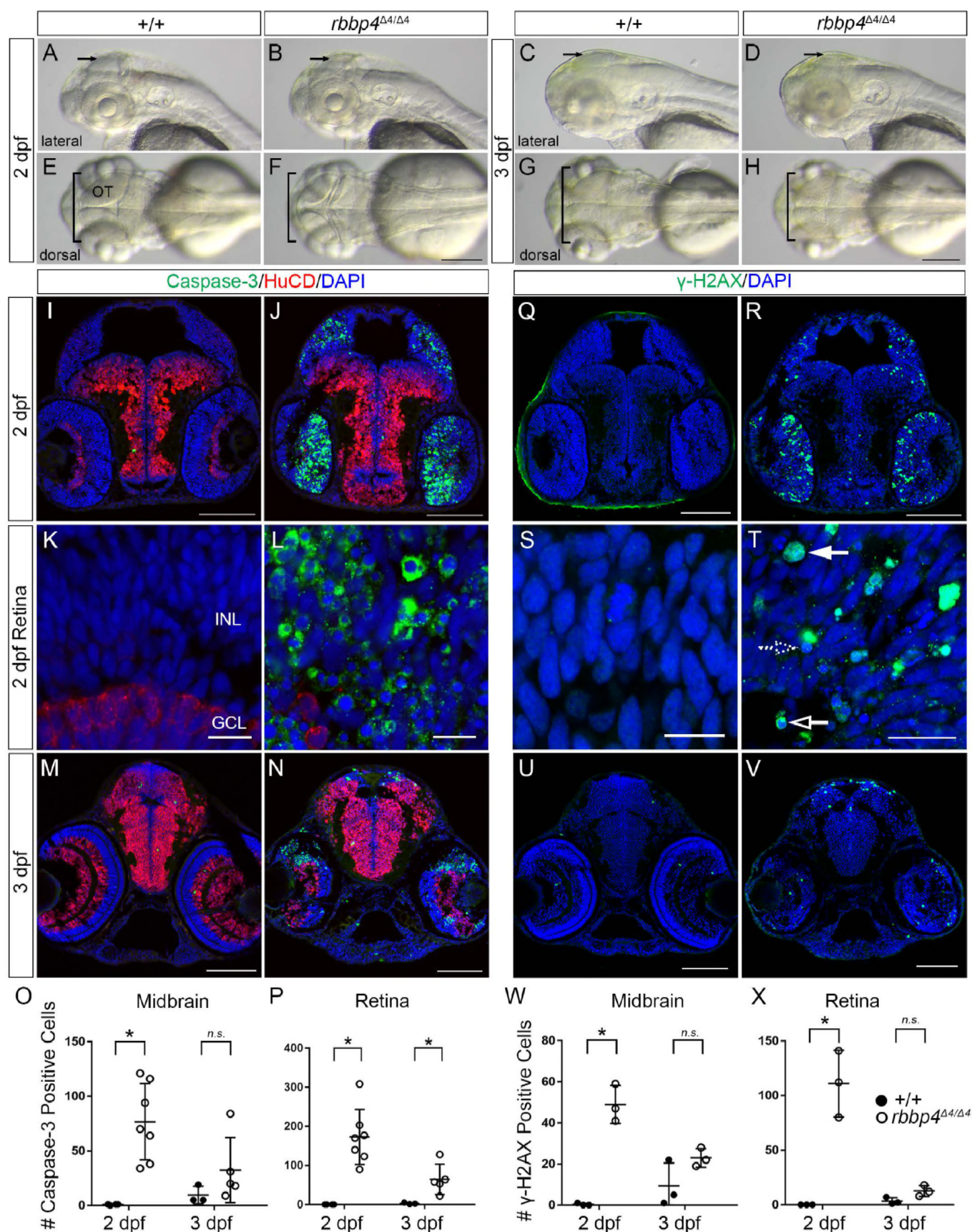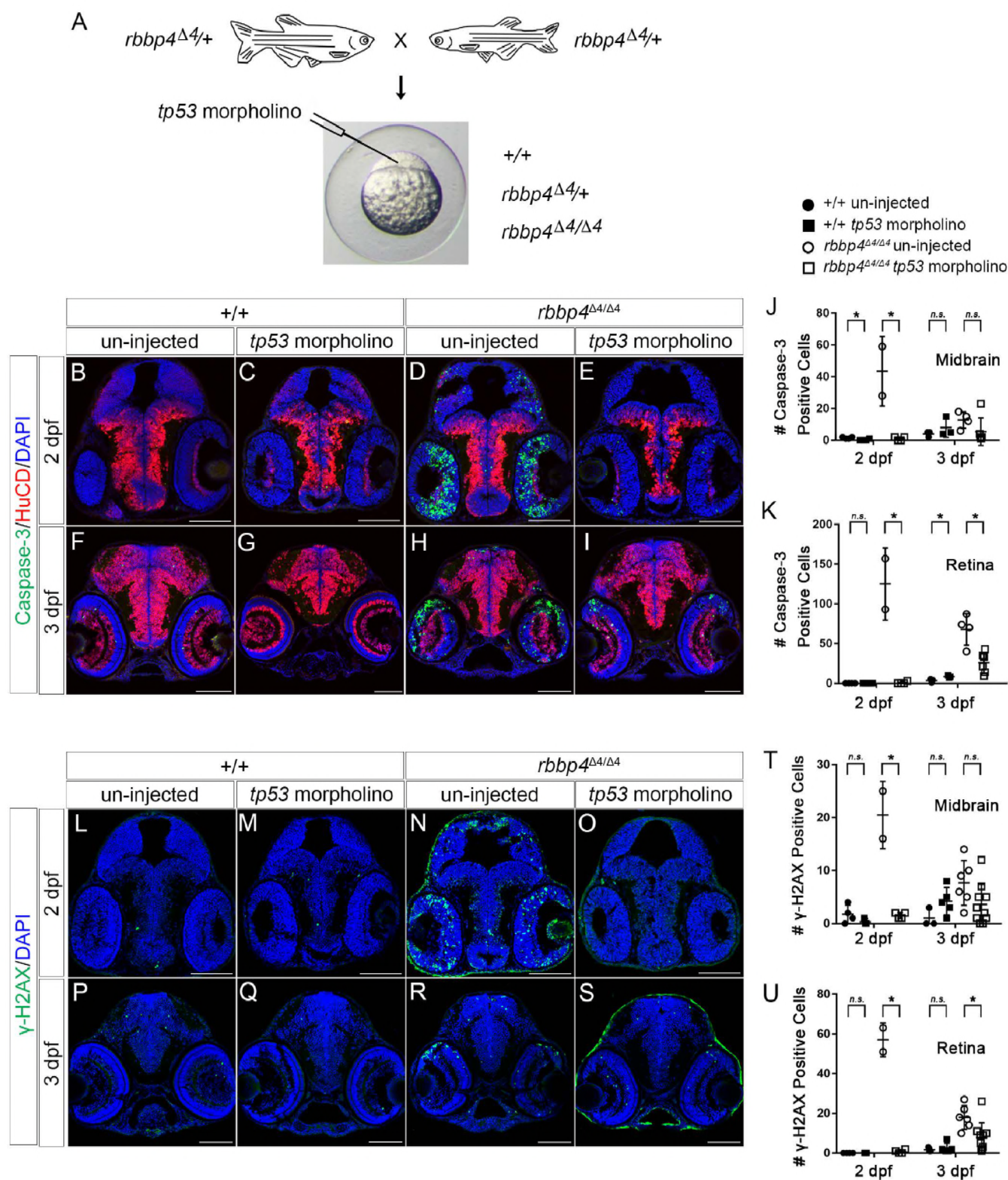
Fig 5. Tp53-dependent activation of DNA damage response and apoptosis in *rbbp4Δ4/Δ4* **mutant neural precursors.**
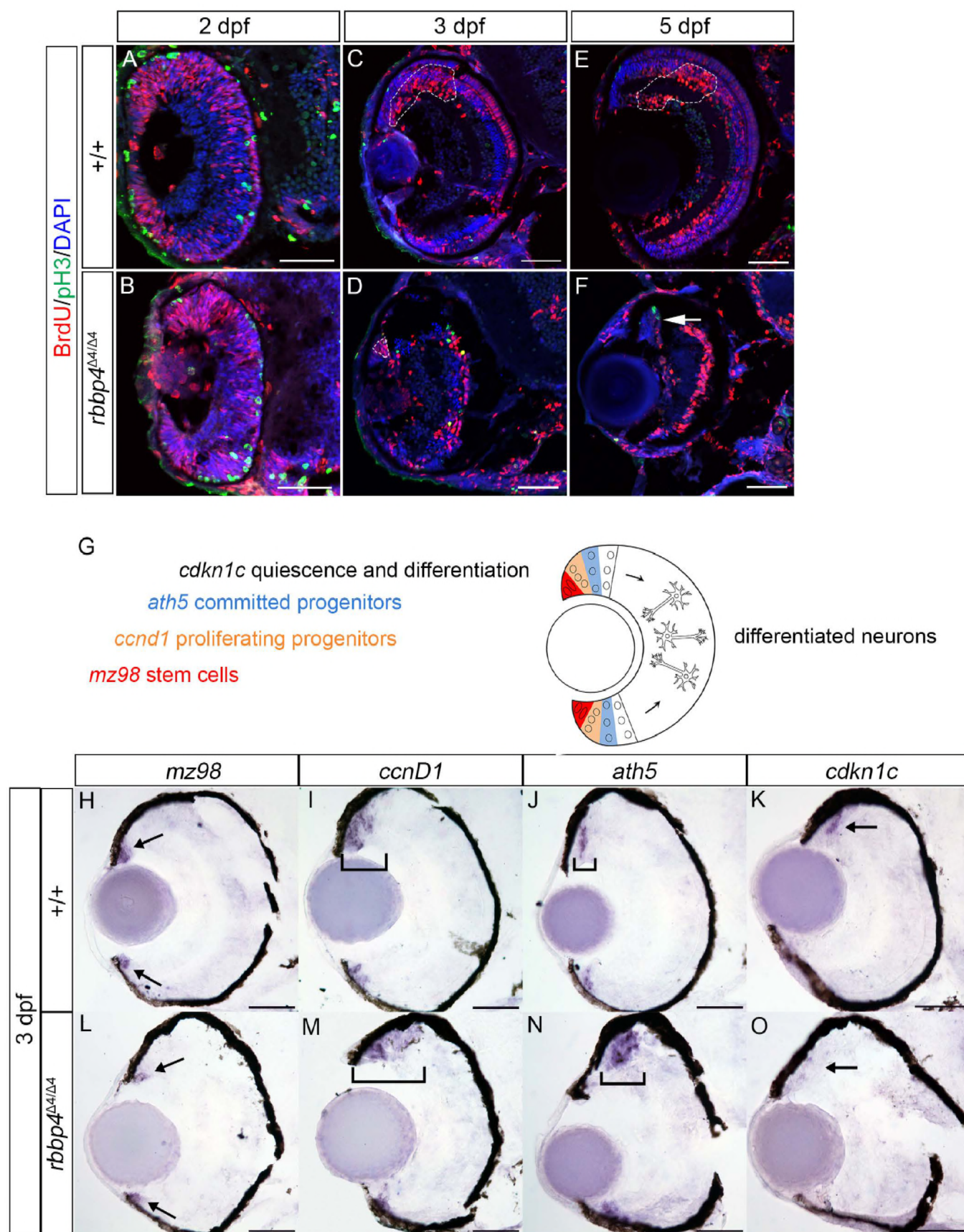
Fig 6. Neural precursors fail to survive and initiate quiescence and differentiation in *rbbp4Δ4/Δ4* **homozygous mutant retina.**
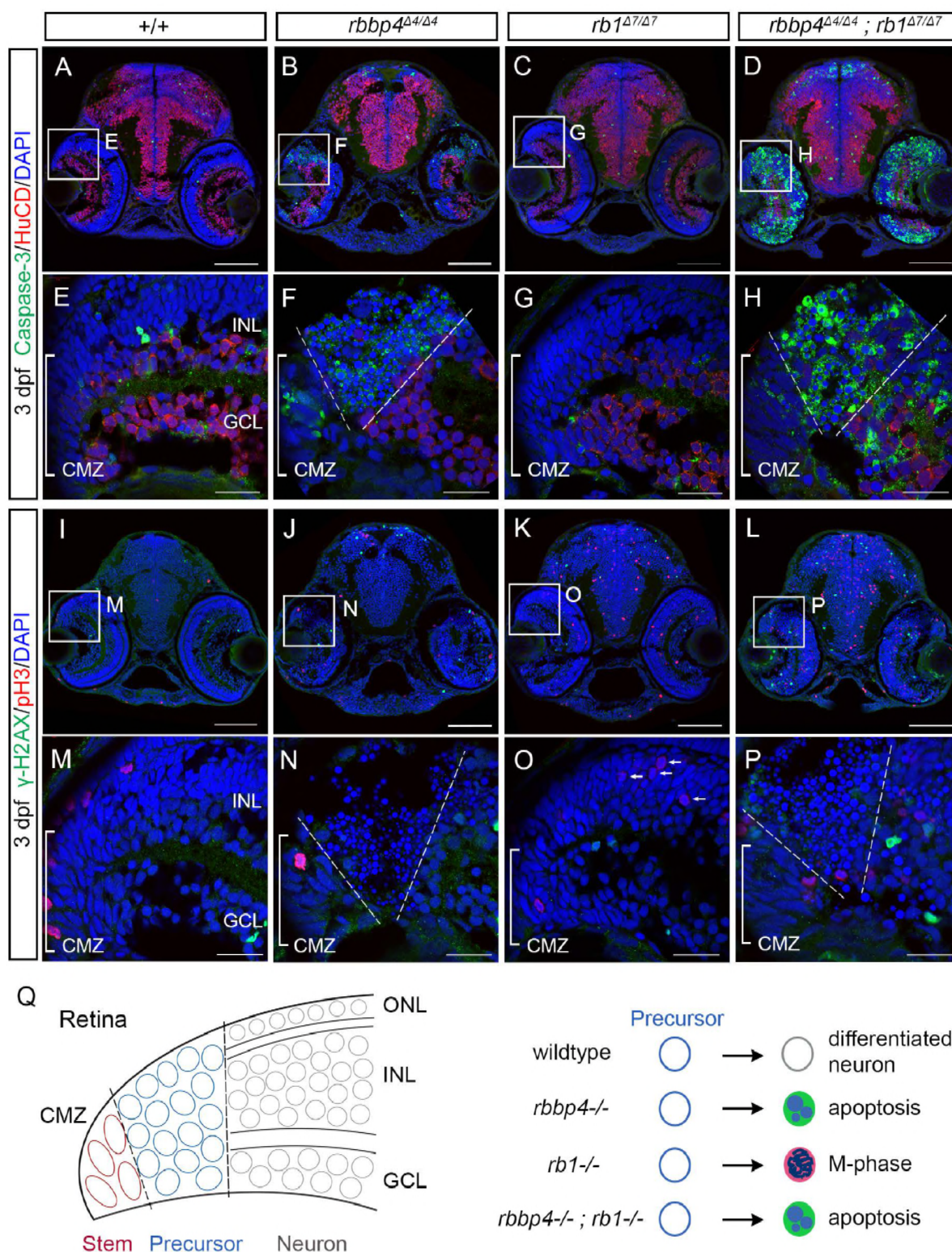
Fig 7. Rbbp4 is required for survival of *rb1-/-* mutant retinal neural precursors.
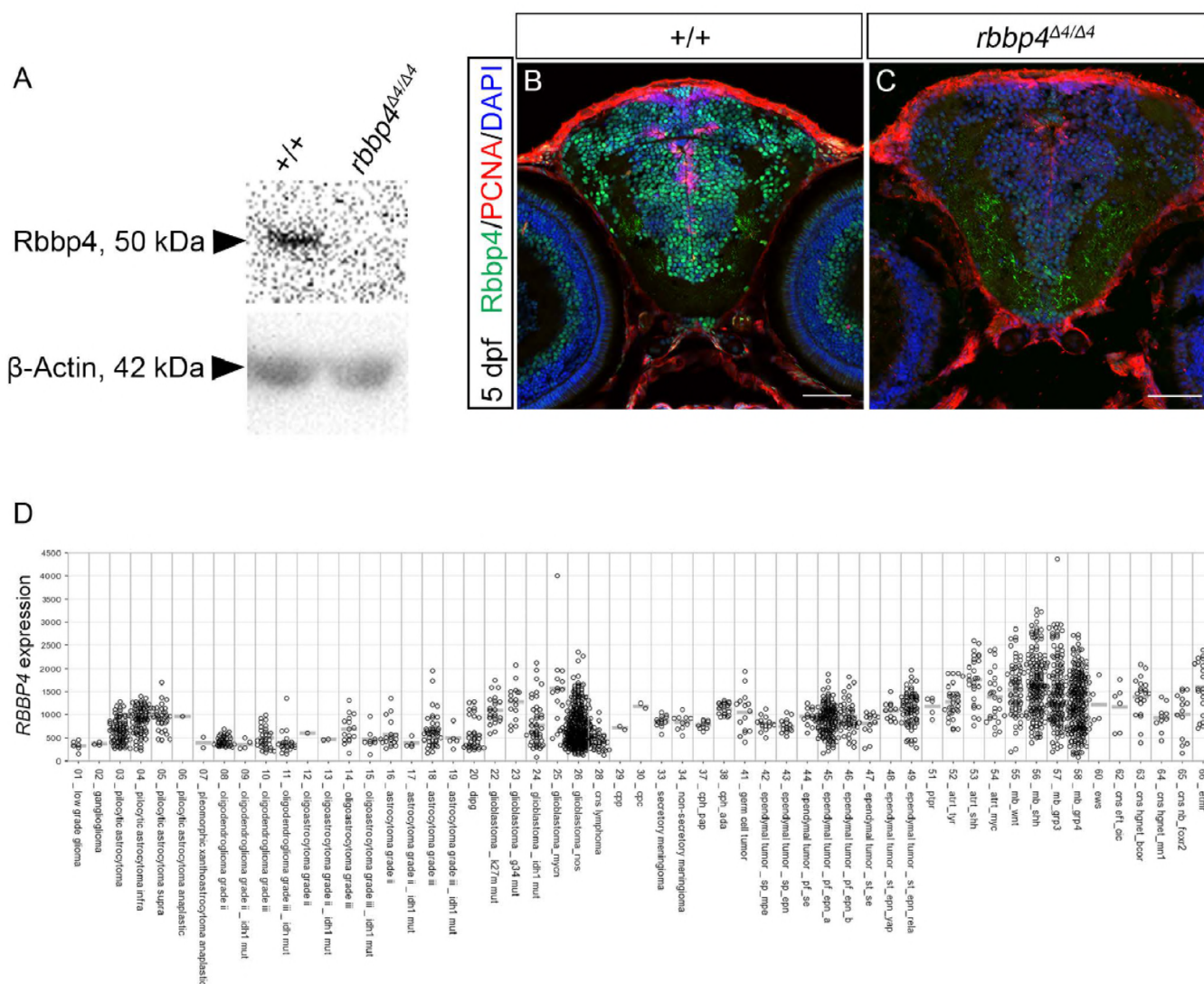
Figure S1. Related to Figures 1 and 2. (A-C) Rbbp4 protein is absent in *rbbp4Δ4/Δ4* homozygous mutant larvae at 5 dpf. (A) Western blot of whole protein lysate from wildtype +/+ and homozygous mutant r*bbp4Δ4/Δ4* 5 dpf larvae probed with a rabbit polyclonal anti-Rbbp4 antibody. The antibody recognizes a single polypeptide band of ~50kDA, close to the Rbbp4 predicted size of 48kDa. The band is absent from the *rbbp4Δ4/Δ4* mutant protein extract. Lower panel, loading control blot probed with mouse monoclonal antibody β-actin. **(B, C)** Rbbp4 and proliferative marker PCNA antibody labeling of transverse sections through the head of 5 dpf wildtype (B) and *rbbp4Δ4/Δ4* homozygous mutant (C) zebrafish larvae. Confocal images for each larva were captured at approximately the same gain settings, with a slightly higher gain setting for the homozygote, to confirm the absence of Rbbp4 signal. In wildtype brain (B) high levels of Rbbp4 are present in the nucleus of neurons in the tectum and thalamic regions, but are nearly absent in the *rbbp4Δ4/Δ4* homozygote (C).Scale bars: 50 μm. **(D) RBBP4 is highly expressed in many human brain tumor entities.** *RBBP4* Affymetrix data from 2284 human tumor samples (German Cancer Research Center DKFZ). atrt atypical teratoid/rhabdoid tumor, cns central nervous system; cpc choroid plexus carcinoma; cph , cpp choroid plexus papilloma; dipg diffuse intrinsic pontine glioma; etmr embryonal tumor with multilayered rosettes; ews Ewing's sarcoma; mb medulloblastoma; ptpr papillary tumor of the pineal
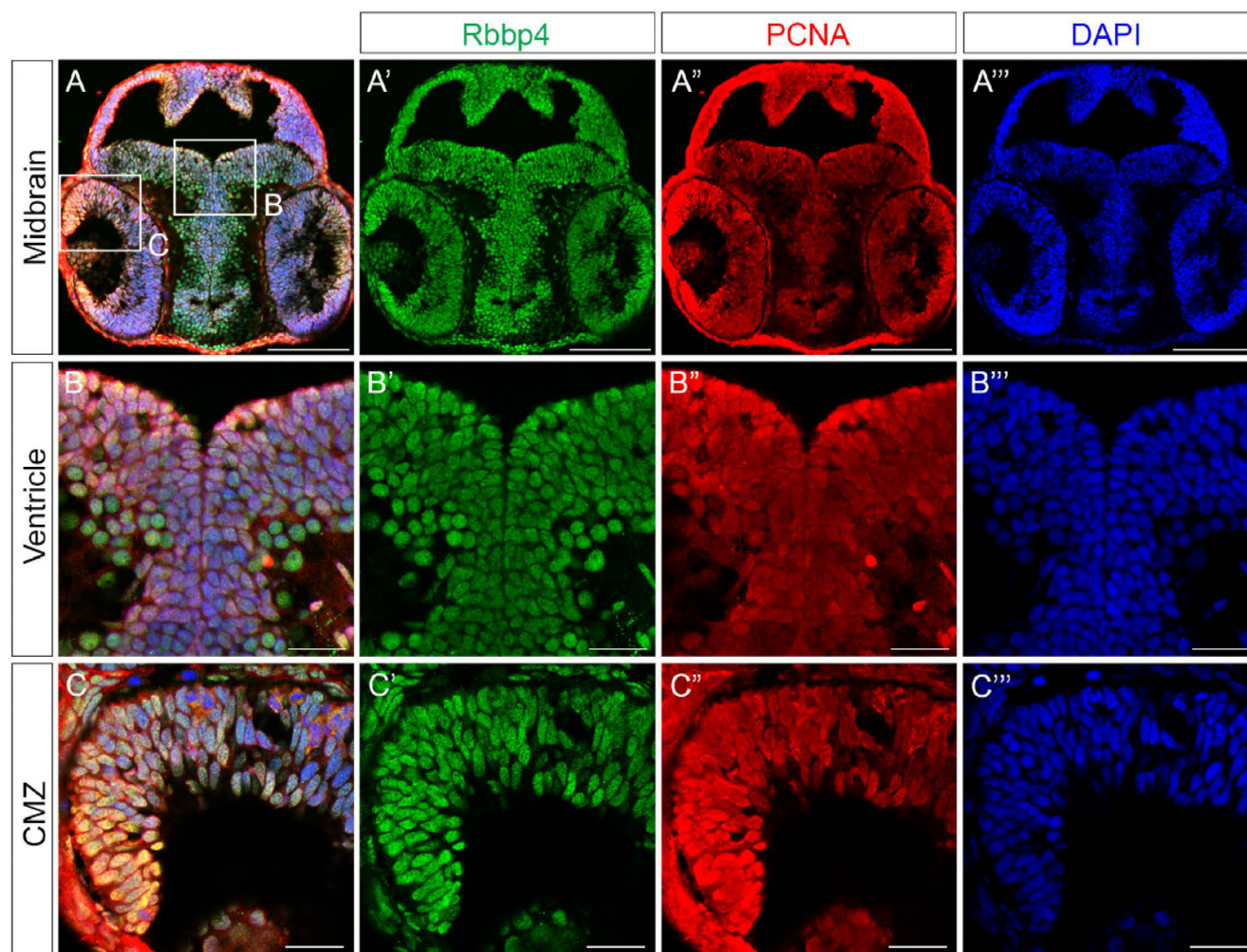
Figure S2. Related to Figure 2. Rbbp4 is ubiquitously expressed in neuroblasts in the embryonic zebrafish brain and retina. (A-A''') Representative transverse cryosections (n=3) through 2 dpf wildtype zebrafish midbrain labeled with antibodies to Rbbp4 (green), proliferation maker PCNA (red), and nuclear stain DAPI (blue). Boxes outline the ventricle at the top of the thalamus in the midbrain (B) and the ciliary marginal zone (CMZ) of the retina (C). (B-B''') Higher magnification view of the midbrain ventricle at the thalamus. (C-C''') Higher magnification view of the ciliary marginal zone of the retina (C-C'''). Scale bars: 100 µm A-A'''; 20 µm B-C'''.
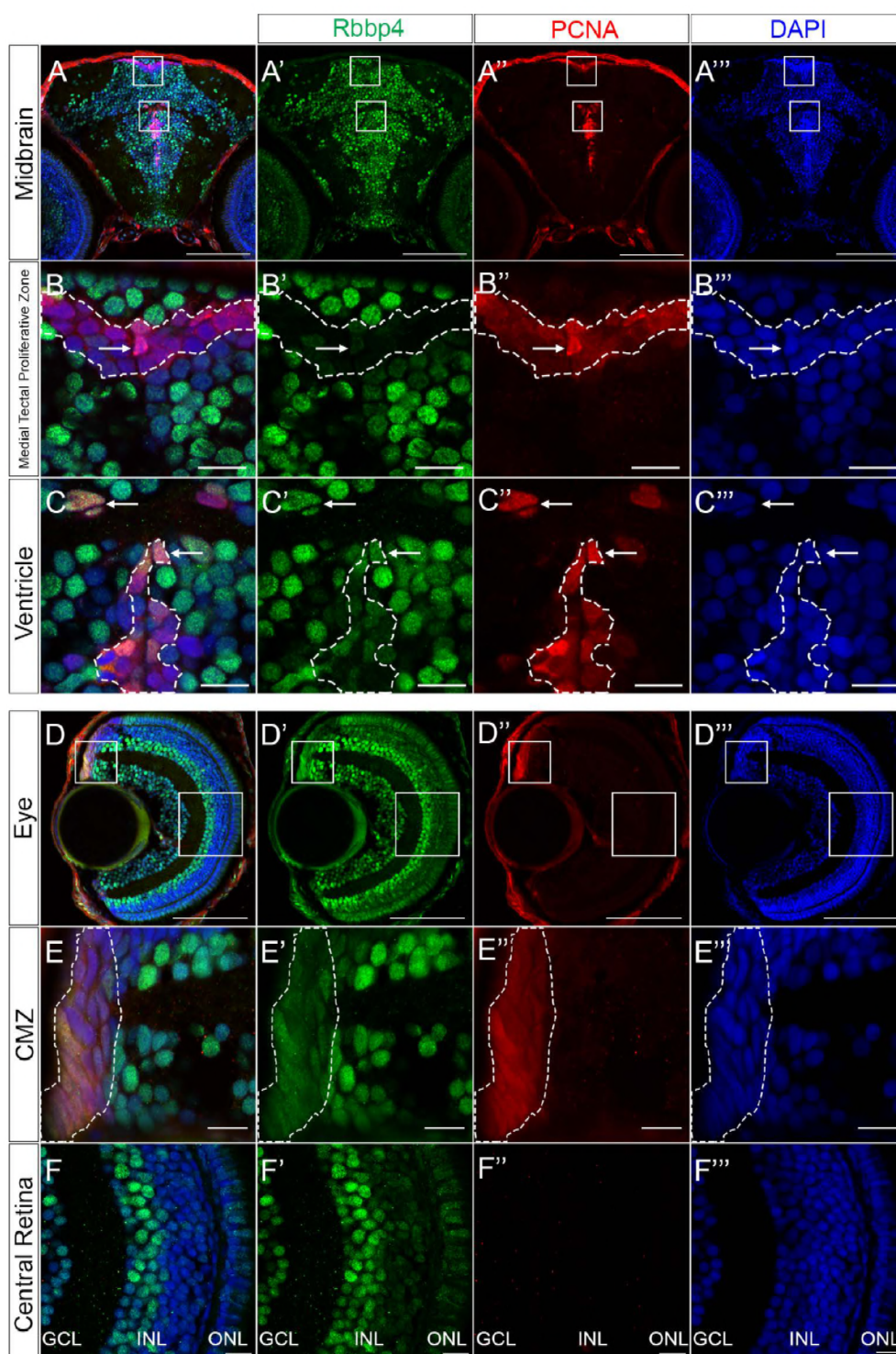
Figure S3. Related to Figure 2. Rbbp4 levels vary in neural stem cells, precursors and neurons in the larval zebrafish brain and retina. Representative transverse cryosections (n=3) of 5 dpf wildtype zebrafish midbrain (A-A''') and retina (D-D''') labeled with antibodies to Rbbp4 (green), proliferation maker PCNA (red), nuclear stain DAPI (blue). Higher magnification view of the medial tectal proliferative zone (B-B'''), brain ventricle (C-C'''), ciliary marginal zone (E-E'''), and central laminated layers of the retina (F-F'''). The highly proliferative, PCNA+ population of cells are outlined; arrows indicate cells co-labeled with Rbbp4 and PCNA. Rbbp4 is enriched in a subset of neurons in the midbrain and vitreal side of the retinal inner nuclear layer. GCL, ganglion cell layer; INL, inner nuclear layer; ONL, outer nuclear layer. Scale bars: 100 µm A-A''', D-D'''; 10 µm B-B''', C-C''', E-E''', F-F'''.
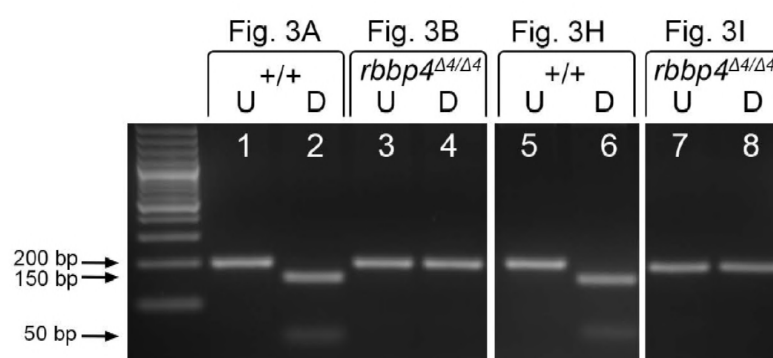
Figure S4. Related to Figure 3. Genotype confirmation of progeny from *rbbp4Δ4/Δ4 ; Tg(Tol2<ubi:rbbp4-2AGFP>)* rescue experiment. A 196 bp PCR amplicon surrounding *rbbp4* exon 2 containing the 4 bp deletion mutation that overlaps a *Sml*I restriction enzyme site. (Lanes 1, 2, 5, 6) *Sml*I digestion of +/+ wildtype larva (Fig. 3A) and transgenic +/+ larva (Fig. 3H) generates 150 and 46 bp fragments. (Lanes 3, 4) In homozygous *rbbp4Δ4/Δ4* larvae (Fig. 3B) the *rbbp4Δ4* allele is resistant to digestion. (Lanes 7, 8) The resistant band in lane 8 confirms the *Tg(Tol2<ubi:rbbp4-2AGFP>)* rescued larva (Fig. 3I) is homozygous for the *rbbp4Δ4* allele. U, un-digested; D, *Sml*I digested. (B-Q)
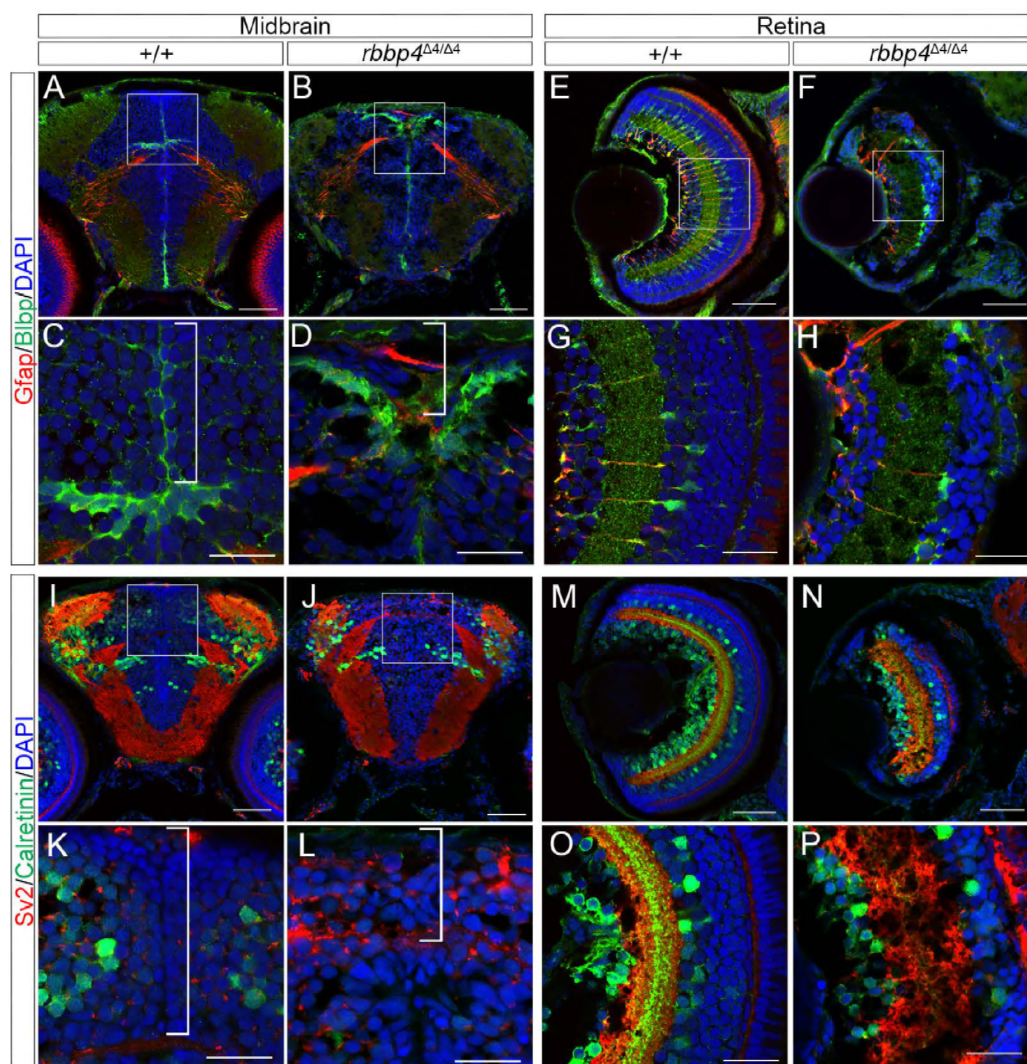
Figure S5. Related to Figure 3. Maternal Rbbp4 allows early born neurons and glia in *rbbp4Δ 4/Δ4* homozygotes to undergo normal neurogenesis and differentiation. Transverse section of midbrain and retina from wild type +/+ (n=3) and *rbbp4Δ4/Δ4* homozygous (n=3) 5 dpf larva labeled with antibodies to glial markers Gfap (red) and Blbp (green) and nuclear stain DAPI (blue). (A, C) In wild type midbrain Blbp and Gfap label radial glia cell bodies and projections in the tectum (C bracket) and thalamic regions, respectively. (B, D) The *rbbp4Δ4/Δ4* mutant midbrain contains mature radial glia in the thalamic region (B). Intense Blbp labeling is present where hypertrophic stem cells are located at the ventricle (D bracket). (E, G) Blbp and Gfap label Mueller glia cells bodies and projections across the inner plexiform layer of the wild type retina. (F, H) Blbp and Gfap label persists in early born glia in the *rbbp4Δ4/Δ4* mutant retina. (I-P) Transverse section of midbrain and retina from wild type +/+ (n=3) and *rbbp4Δ4/Δ4* mutant (n=3) 5 dpf larvae labeled with antibodies to the synaptic vesicle marker Sv2 (red) and interneuron and ganglion cell marker Calretinin (green) and nuclear stain DAPI (blue). (I, K) In wildtype brain, Sv2 labels the neuropil, and Calretinin labels the cell bodies of a subset of mature neurons in the thalamus and tectum (K bracket). (J, L) The *rbbp4Δ 4/Δ4* mutant shows a reduction in the tectal neuropil and number of Calretinin-positive neurons (L bracket). (M, O) Sv2 and Calretinin labeling in wild type retina. (N, P) Early born neurons maintain Calretinin labeling and Sv2 labeled projections across the inner and outer plexiform layers in the *rbbp4Δ4/Δ4* mutant retina. Scale bars: 50 μm A, B, E, F, I, J, M, N; 20 μm C, D, G, H, K, L, O, P.
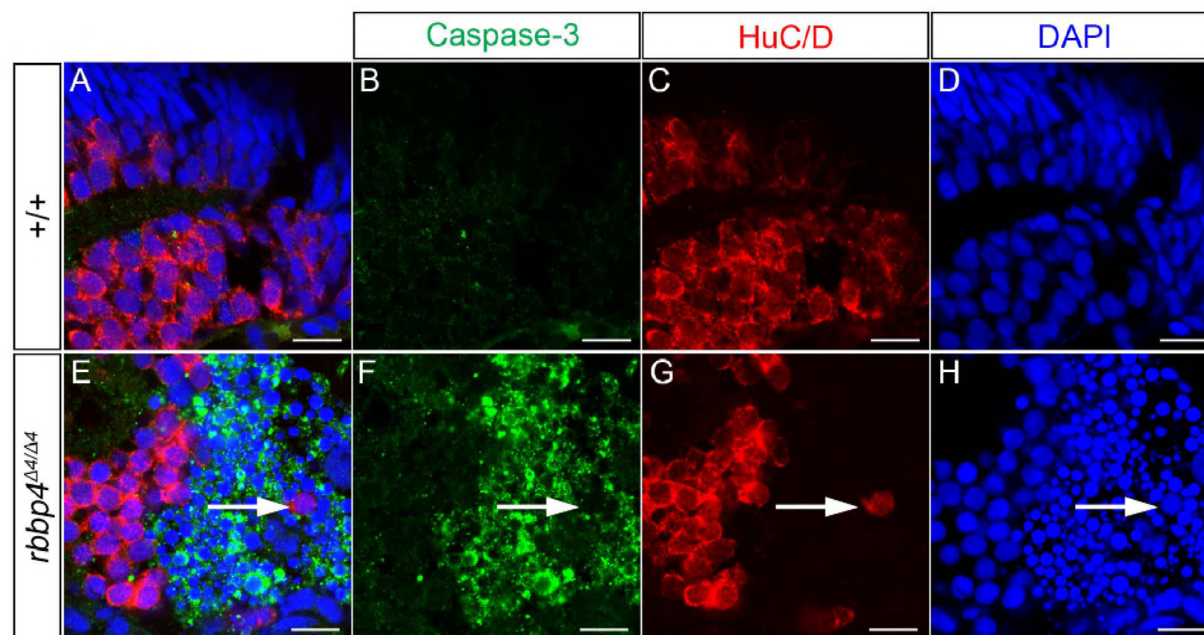
Figure S6. Related to Figure 4. Caspase-3 labeled *rbbp4Δ4/Δ4* **mutant retinal cells undergoing apoptosis do not express the neuronal marker HuC/D.** (A-H) Transverse sections of 3 dpf zebrafish retinas labeled with antibodies to the apoptosis marker activated Caspase-3 (green), neuronal marker HuC/D (red), and nuclear stain DAPI (blue). (A-D) In wildtype +/+ HuC/D is detected in neuron cell bodies in the inner nuclear layer and photoreceptor layer of the retina. (E-H) In the *rbbp4Δ4/Δ4* homozygous retina cells expressing activated Caspase-3 do not co-label with HuC/D. Arrow points to an activated Caspase-3-negative/HuC/D-positive cell surrounded by activated Caspase-3-positive/HuC/D-negative cells. Scale bars: 100 μm.
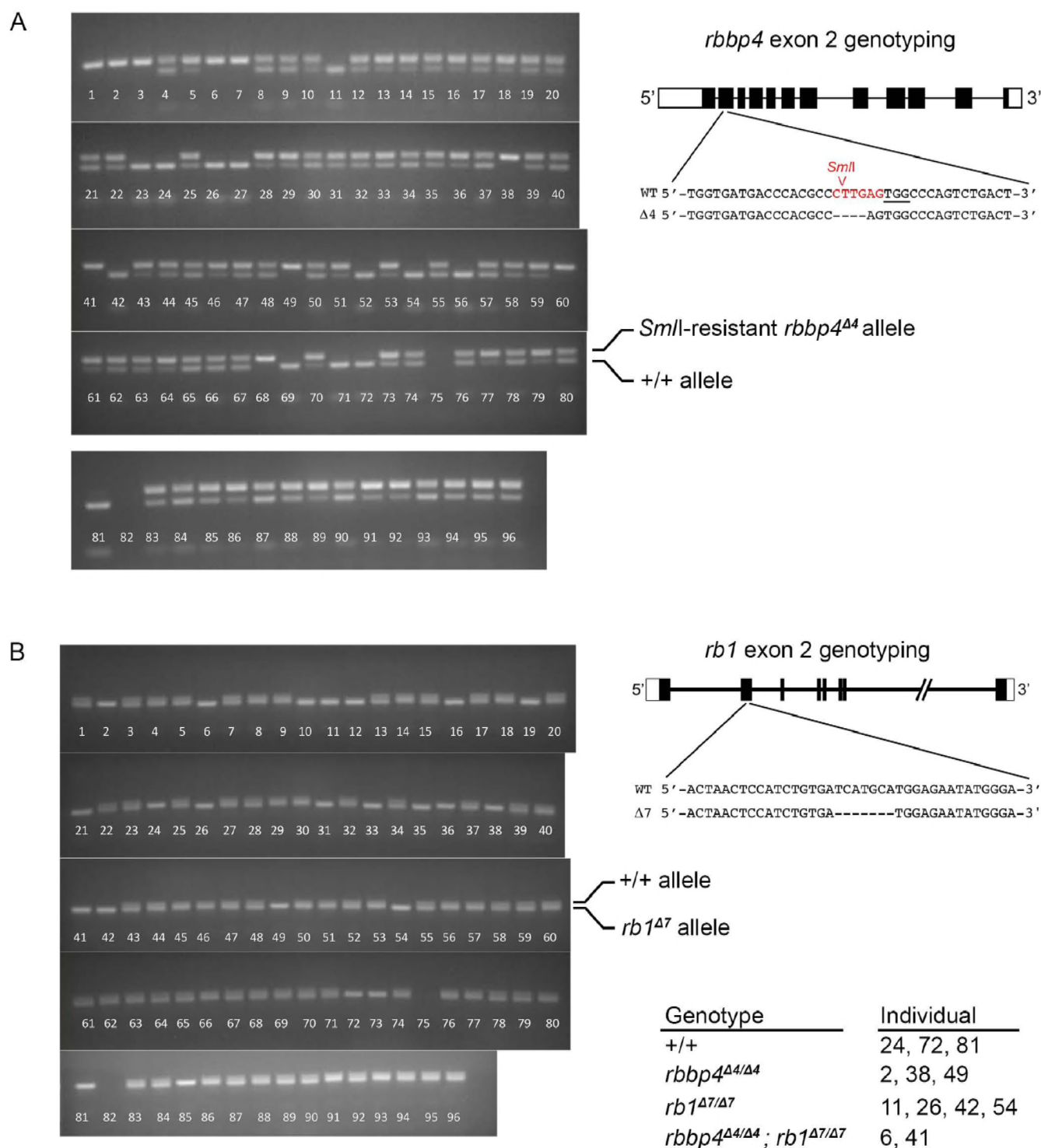
Figure S7. Related to Figure 7. PCR genotyping to confirm genotype of +/+ wildtype, *rbbp4*$^{Δ4/Δ4}$ mutant, *rb1*$^{Δ7/Δ7}$ mutant, and *rbbp4*$^{Δ4/Δ4}$; *rb1*$^{Δ7/Δ7}$ double mutant 3 dpf larvae from *rbbp4*$^{Δ4/+}$; *rb1*$^{Δ7/+}$ double heterozygous incross. Each lane corresponds to an individual progeny. A Gels of *rbbp4* exon 2 PCR amplicons digested with *Sml*I. The digestion-resistant bands correspond to the *rbbp4*^{Δ4} allele. **B** Gels of *rb1* exon 2 PCR amplicons. The 7bp deletion and wildtype alleles can be distinguished based on band size.

S1 Table. Frequency of progeny classes by genotype and phenotype from heterozygous *rbbp4Δ4/+* crossed to heterozygous *rbbp4Δ4/Δ+ ; Tg(Tol2<ubi:rbbp4-2AGFP>)* adults.

Cross	Total # of progeny	GFP Negative						GFP Positive					
		Total GFP-	Normal Phenotype	Mutant Phenotype	rbbp4 +/+	rbbp4Δ4/+	rbbp4Δ4/Δ4	Total GFP+	Normal Phenotype	Mutant Phenotype	rbbp4 +/+	rbbp4Δ4/+	rbbp4Δ4/Δ4
Clutch 1	76	39/76 (51.3%)	28/39 (71.8%)	11/39 (28.2%)	n/a	n/a	n/a	37/76 (48.7%)	37/37 (100%)	0/37 (0%)	8/37 (21.6%)	17/37 (45.9%)	12/37 (32.4%)
Clutch 2	108	61/108 (56.4%)	48/61 (78.6%)	13/61 (21.3%)	5/24 (20.8%)	11/24 (45.8%)	8/24 (33.3%)	47/108 (43.5%)	47/47 (100%)	0/47 (0%)	8/24 (33.3%)	11/24 (45.8%)	5/24 (20.8%)
Clutch 3	307	155/307 (50.5%)	110/155 (71%)	45/155 (29%)	18/48 (47.3%)	17/48 (35.4%)	13/48 (27%)	152/307 (49.5%)	152/152 (100%)	0/152 (0%)	16/48 (33.3%)	22/48 (45.8%)	10/48 (20.8%)

S1 Table. Related to Fig 3. Frequency of progeny genotypes and phenotypes from heterozygous *rbbpΔ4/+* crossed to heterozygous *rbbpΔ4/+;Tg(Tol2<ubi:rbbp4-2AGFP>)* zebrafish. Three independent crosses were set up between female rbbpΔ4/+ heterozygotes and male *rbbpΔ4/+;Tg(Tol2<ubi:rbbp4-2AGFP>)* transgenic heterozygotes. Embryo clutches were sorted into positive and negative GFP groups at 2dpf. At 5dpf larvae were sorted by phenotype and then genotyped. "Total" column shows approximately 50% GFP- and GFP+ in each clutch, indicating the *Tg(Tol2<ubi:rbbp4-2AGFP>)* line contains a single transgene integration. Scoring of GFP negative embryos revealed close to Mendelian segregation of the *rbbpΔ4/Δ4* gross mutant phenotype in one quarter of the progeny (28.2%, 21.3%, 29%). A random sampling of embryos from clutches 2 and 3 were genotyped and confirmed Mendelian segregation of the phenotype with the rbbpΔ4 allele. In each clutch, none of the GFP positive embryos showed the rbbp4 mutant phenotype. Random sampling and genotyping confirmed ~ one quarter of morphologically normal GFP+ larvae were homozygous mutant *rbbpΔ4/Δ4* (32.4%, 20.8%, 20.8%).

S2 Table. Sequences of primers used in this study.

Oligonucleotides	Forward 5'-3'	Reverse 5'-3'	
rbbp4$^{\Delta 4is60}$ exon 2 allele genotyping primers	GCGTGATGACAGATCTCATATTGTTTTCCC	CTGGTGACATCTGGCAACCACT	Schultz et al., 2018
rb1$^{\Delta 7is54}$ exon 2 allele genotyping primers	TTTCCAGACACAAGGACAAGGATCC	GCAGATATCAGAAGAAAGAGTACATTTGTCTT	Solin et al., 2015
rbbp4 cDNA	catgTCTAGATGTGGAGTCGTTATGGCTG	catgGGATCCTCCCTGAACCTCAGTGTCTG	This paper.
mz98 cDNA	CCGGACACTACACACTCAATGC	GTGCTGGATGTAGCTGTTCTCG	This paper.
ccnD1 cDNA	GCGAAGTGGATACCATAAGAAGAGC	GCTCTGATGTATAGGCAGTTTGG	This paper.
ath5 cDNA	GATTCCAGAGACCCGGAGAAG	CAGAGGCTTTCGTAGTGGTAGGAG	This paper.
cdkn1c cDNA	CGTGGACGTATCAAGCAATCTGG	GTCTGTAATTTGCGGCGTGC	This paper.